LASER INDUCED FLUORESCENCE GAS PUFF DENSITY MEASUREMENTS

A Thesis

Presented to the Faculty of the Graduate School

of Cornell University

in Partial Fulfillment of the Requirements for the Degree of

Master of Science

by

Matthew Thomas Evans

August 2012

ABSTRACT

The double gas puff valve is a device used to inject a supersonic puff of gas to act as a load in z-pinch plasma implosions. The purpose of the annular gas shells is to mimic a cylindrical column along the z-axis in efforts to reduce Rayleigh-Taylor instability. However before integration of the valve into the z-pinch pulsed power machine the gas profile needs to be examined. Tuning the density of the gas to fit specific profiles leads to improvement in plasma radiative sources and yields. The axial uniformity of the cylindrical gas column is highly dependent on the nozzle characteristics and shape. Performance is then determined by the density, speed, and symmetry of the gas column. Measurement of the density distribution is performed using a spectroscopic measuring technique called laser-induced fluorescence. LIF is a 1-dimensional imaging technique that maps the concentration of atoms with the aid of a tracer. LIF and the 2-dimensional counterpart planar laser-induced fluorescence (PLIF) examine the gas flow in the r-z plane with sub-millimeter resolution. The tracer molecule fluoresces due to excitation by a laser beam. The fluorescence signal is imaged using a streak camera and a charge-coupled-device (CCD) in combination. The method also allows the study of gas puff reliability. Any differences between gas shells can then be examined and interpreted with reliable certainty. Imaging software is used to determine the density from the intensity of the fluorescence images. A detail account of the process is illustrated in this study. A control system was constructed for operations of the gas puff valve in both LIF and z-pinch experiments. The pressure system is designed to tailor specific profiles as needed. The LIF system is detailed along with any components built for

the gas puff valve. Results of these measurements serve to verify the uniformity of flow and determine the density distribution of the gas puff.

BIOGRAPHICAL SKETCH

Matthew Thomas Evans was a Master student in the Applied Physics program at Cornell University from August 2010 to August 2012.

This document is dedicated to all Cornell graduate students.

ACKNOWLEDGEMENTS

This dissertation was made possible by the contributions of several individuals. I would like to thank Dr. Bruce Kusse, Dr. Niansheng Qi, Dr. Pierre Gourdain, Harry Wilhelm, Todd Blanchard, Cad Hoyt, and Adam Cahill.

TABLE OF CONTENTS

LIST OF FIGURES

CHAPTER 1

INTRODUCTION

The goal of this study is to characterize and control the z-pinch gas puff load from an electromagnetic fast acting valve. The valve produces two concentric annular gas shells with density of several $\mu g/cm^3$. Fast opening gas puff valves are a common way to produce a supersonic gas puff for z-pinch experiments. Gas puff z-pinch plasmas are intense sources of x-ray radiation with applications in inertial confinement fusion energy and characterization of materials. In pulsed power z-pinch experiments, stable implosions are crucial and understanding the gas dynamics of the system improves x-ray yield. A pulse of gas ejected at supersonic speeds propagates along the z-axis with limited radial expansion. Profiling the gas density distribution requires a system that can measure sub-millimeter gas concentrations on a microsecond time scale. The 1-dimensional gas density profile of the puff was measured using Laser-Induced-Fluorescence (LIF). The construction of a LIF system and the relative density profile measurements of the gas puff loads are the focus of this thesis. The principles of LIF and the gas puff valve are detailed in Chapter 2. The operation of the gas puff load and the control system are described in Chapter 3. The optical system required for LIF measurements can be altered to examine a 2-dimensional gas density profile. The thesis also provides proof of concept for Planar Laser Induced Fluorescence (PLIF) measurements and illustrates a few example images. The resulting density profiles and associated images are examined in Chapter 4.

1.1 Motivation and Application

At Cornell University z-pinch plasma studies are performed on the COrnell Beam Research Accelerator (COBRA) a 1 MA, 100-200 ns pulsed power driver. COBRA studies have been widely involved with fine metal wire array loads and radial/cylindrical metal foil load, which bridge the anode-cathode gap. Research has been shown that replacing metal wires with a neutral gas can also produce intense x-ray plasma radiation sources [1]. The neutral gas acts as a resistive load through which the 1 MA current passes from the anode to cathode. The high voltage potential difference between the anode and cathode causes an electrical breakdown in the A-K gap. The breakdown voltage is a function of the distance between the anode and cathode and the pressure of the neutral gas, where a fast acting gas puff valve is used to inject supersonic puffs into the load region. Then the gas load undergoes a z-pinch implosion and forms a hot dense pinched plasma.

One of the challenges in z-pinch implosions is to reduce the Rayleigh-Taylor (RT) instability. RT instability is a common fluid instability that occurs when a heavier fluid is placed on top of a lighter fluid in a constant gravitational field. The equilibrium between the two fluids is unstable causing perturbations to grow. In imploding plasma such as a z-pinch, RT instabilities occur at the interface between the plasma (lighter fluid) and the azimuthal magnetic field (heavy fluid). RT instability has a known negative effect on z-pinch radiation sources. Perturbations that grow along the plasma surface release potential energy that reduces the x-ray yield [2].

In z-pinch experiments, there is a general amount of variation between each

shot fired [3]. The large variation of the z-pinch implosion between shots could be the result of the pulsed power driver or the plasma itself. Reproducibility is often a serious problem in large scale pulsed plasma experiments. Eliminating variation in the load or the machine itself can help produce more good shots than bad. Currently COBRA is capable of firing approximately three shots per day, limited by loading time and accelerator cool down. Loading time consists of constructing a physical wire array and placing it in the anode-cathode gap. The vacuum chamber then needs about two hours to pump down and reach the high vacuum of 10^{-5} torr. Replacing the solid wire array load with a gas puff eliminates wire array replacement time and the need to open the vacuum chamber between shots. Thus, the limiting factor of the shots then becomes the machine cool down time. The reduction in time would allow for an increase in shots per day, at the suggested amount of 4-5, which is about 30 to 60% increase of the previous runs. The increased shot rate results in a larger data set during an experimental run. The gas puff valve is currently capable of firing over 100 shots before maintenance services [4]. If properly maintained the gas puff z-pinch load should be able to last two full two-week runs without the need for repairing or alteration.

Adding z-pinch gas puff capability to COBRA does require a great deal of effort, since the timing and constructions of the gas puff valve system must be precise for shot-to-shot reproducibility. Variation in the amount of gas injected by the valve could cause shot-to-shot variation of the plasma density and implosions. Valve heating is not a concern for an actual COBRA shot since the valve "cool down" time is on the order of minutes where time between shots is hours. The gas valve output is dependent upon the current used to the pulse the valve and is reported in this study.

1.2 High Energy Density Plasmas (HEDP)

Laboratory high energy density plasma experiments are limited by the scale of facilities and devices used to generate the plasma. Self-constricted plasma configurations are desirable since the aim of the system is to use the plasma to confine itself. Additional equipment needed to stabilize the plasma is not necessary. The two most common ways to create a plasma confinement system are using high energy/power lasers or pulsed power fast z-pinch accelerators. The current from a pulsed power accelerator implodes a load to extreme states of density and temperature. The interaction of this matter with itself, particle beams and radiation fields is referred to as high energy density physics (HEDP) [5].

High energy density refers to energy densities exceeding 10^{11} joules per cubic meter or pressures exceeding 1 megabar. Applications of HEDP generally focus on inertial confinement fusion and astrophysics. Inertial confinement fusion is where a fuel target is compressed and heated to invoke nuclear fusion reactions. The goal of inertial confinement is to start a fusion explosion with an energy gain of 100 [5]. Both high power lasers and pulsed power drivers are used to start the initial fusion reaction and research in this field continues today. Replicating astrophysical phenomena is a great source of interest in HEDP experiments. For z-pinch experiments large fluxes of x-rays at energies of a few keV can be useful for radiation transport experiments. A conical wire array or Al foil z-pinch produces a jet of material that radiatively collapses. These jets are relevant to astrophysical jets in HED regimes. A greater comparison between theory and experimental work can be achieved. Spin-off technology such as high speed instrumentation, high-power lasers, advanced pulse power

and microfabrication techniques are developed in the field to aid in advancing HEDP research.

1.3 Z-pinch and gas puff load

A Bennett pinch or z-pinch is the simplest static equilibrium that produces a dense hot plasma [4]. A z-pinch consists of an axisymmetric cylindrical plasma with axial current J and no other currents. The z refers to the direction of current along the cylinder axis. In pulsed plasma experiments a z-pinch is produced by applying a fast current pulse across the anode-cathode gap. Typically the load is setup in a cylindrical shell geometry made of a metal wire array or a gas column. The current density J flows on the surface of the cylinder. An azimuthal magnetic field B curls around cylinder. This creates a Lorentz force (JxB) directed inwards to the center. The Lorentz force overcomes the hydrodynamic pressure that pushes outward. The kinetic and magnetic field energies are converted to thermal energy as the plasma implodes creating a hot dense core at the center that provides a radiative pulse. During the implosion the plasma is unstable and quickly expands. The z-pinch is illustrated below in figure 1.1.

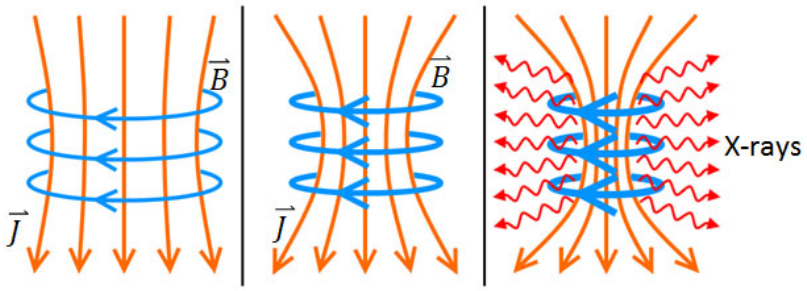

Figure 1.1: Z-pinch.The current (orange) create an azimuthal magnetic field (blue). The magnetic field pinches inwards along the axis. The plasma implodes and releases x-rays (red) outward [6].

The gas valve produces a gas puff at supersonic speeds. The flow of gas lasts on the order of milliseconds and is turbulent. The shell-on-shell interaction produces large axial and radial gradients. The X-ray output, efficiency and implosion instabilities of z pinches depend on the density and current profiles [7]. Determining the mass distribution of the gas load becomes an essential task in improving z-pinch experiments. Since the plasma behavior is sensitive to the gas valve output it is important to have a reproducible density profile [3]. Low yield gas puff z-pinch experiments are the results of poor estimates of the gas density profile [8]. Poor estimates and timing of the gas puff can also cause stress on the pulsed power machine resulting in damage. In order to improve upon the gas puff z-pinch performance it is essential to characterize the initial gas distribution at the time the current pulse is applied. Thus the r-z density profile and the mass ratio between different gas shells for multi-shell gas puff loads are examined. Characterization of gas flow from the nozzle is examined to reduce RT instability for z-pinch experiments. Neon is used for experiments in this thesis since it will be used in future z-pinch experiments at Cornell.

The energy coupling from the pulsed power driver to the z-pinch plasma is determined by the implosion history. Measurements from the initial gas phase, through the MHD implosion phase, to the final pinch phase are needed to understand implosion physics of the z-pinches. These measurements also provide the critical information to refine the theoretical models, so the models can better predict load performance.

Many diagnostics have been developed for the final pinch phase, and the radiated power, x-ray spectrum, temperature, density and size are measured satisfactorily. Laser shearing interferometer and laser wavefront analyzer have

demonstrated that measurements of the plasma density profile and/or load current are possible during the MHD implosion phase. A PLIF technique to determine the neutral density profiles in the initial gas phase is crucial. Development of this technique is a part of the overall effort to create a comprehensive set of instruments to trace the gas/plasma density profiles from the initial radial gas phase to the final pinch phase. The initial gas phase density profile determines the implosion trajectory. The double gas puff provides flexibility in tailoring the initial gas phase density distribution, by being able to independently set the pressure in each of the two plena. The pressure ranges, and associated density profiles, that optimize the x-ray yield, are determined experimentally. In the past, measurements of the gas puff density have been made using 1-D high sensitivity interferometry. The high sensitivity interferometry requires many radial scans to obtain a 1-D density map. Multiple scans are very time consuming and the spatial resolution is typically limited by the number of scans to several mm. Abel inversion, which typically has large uncertainties at small radii, is needed to unfold the interferometry data. LIF measures the gas profiles quickly (several shots) with a high signal/noise ratio, and high spatial resolution (sub-mm). It allows us to study the flow trajectory, azimuthal symmetry of the density, turbulence in the gas flow, and fine structures due to shell-on-shell interactions. This type of information could be washed out in the axial and radial scans required by interferometry.

CHAPTER 2

BACKGROUND

2.1 Gas puff valve

The gas puff valve was designed and constructed by the Weizmann Institute of Science plasma physics group. The puff valve is an electromagnetic fasting acting valve attached with two concentric nozzles shown in figure 2.1. The double gas puff produces two annular gas shells along the center axis. The hollow center nozzle allows a laser beam to be guided axially along the gas shells. The inner/outer diameters of the outer and inner nozzles are 6/4 cm and 3.6/1.4 cm at the nozzle exit plane, respectively. The gas puff contains two independent plenums for the inner and outer nozzle. Separate plenums allow for pressure adjustments to be made independent of each other. Each plenum typically holds a pressure of 0.5-15 psia.

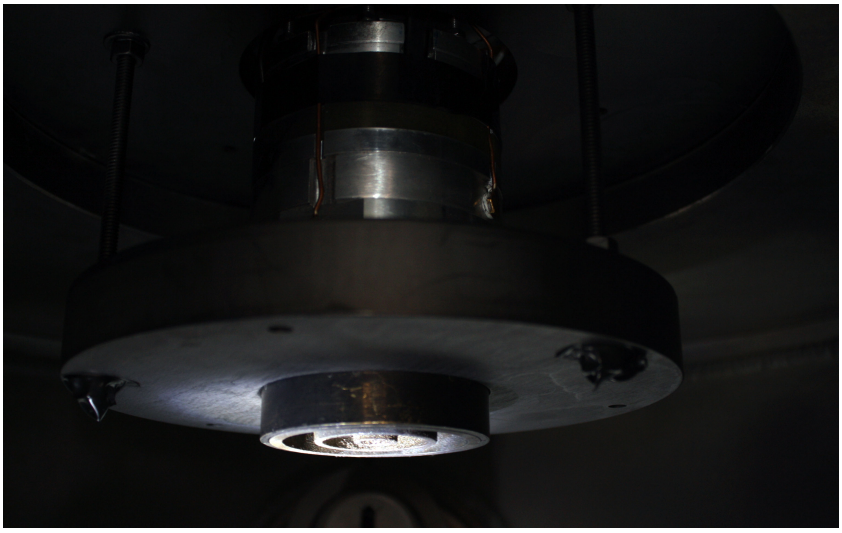

Figure 2.1: Picture of double gas puff valve.

2.1.1 Nozzle

As stated, the gas shell density uniformity is critical in plasma experiments, thus it is important that the dynamics of the nozzle should be analyzed and understood. During z-pinch experiments the plasma implodes radially inwards and stagnates on the axis [9]. The profile linear mass and the rise time of the puff is determined by the geometry of the nozzle [11]. At high supersonic speeds the gas jet has a limited expansion and is uniform azimuthally. If the valve is improperly designed or deformed, gas may expand more radially as it flows along the z-axis. A nonuniform azmimuthal gas density distrubtion makes radial implosion unsymmetrical and can result in unstable plasma before the pinch, producing poor x-ray yields. The production of a supersonic shell of gas is done by a converging-diverging (CD) nozzle. A CD nozzle or de-Laval nozzle is asymmetric hourglass-shape so the exhaust flow is maximally converted into directed kinetic energy [9]. Shown below in figure 2.2 is a diagram of gas flowing through the inner and outer CD nozzle.

The CD nozzle has three sections; a converging section, a throat, and diverging section. The principle of the CD nozzle is to choke the flow of gas at the throat to increase the velocity. To describe the flow of gas in each section we refer to the ranges of the Mach number. The Mach number is a dimensionless quantity that represents the velocity of an object over the speed of sound in that medium. We use the Mach number to describe the velocity of the gas through the nozzle since our goal is to achieve azimuthally uniform and collimated flow propagation that occurs at supersonic speed. Generally gas flow is subsonic ($M < 1.0$) in a conversion chamber. For the speed of the gas to be supersonic ($M > 1.0$) the second chamber must be at a lower pressure, and the gas has to

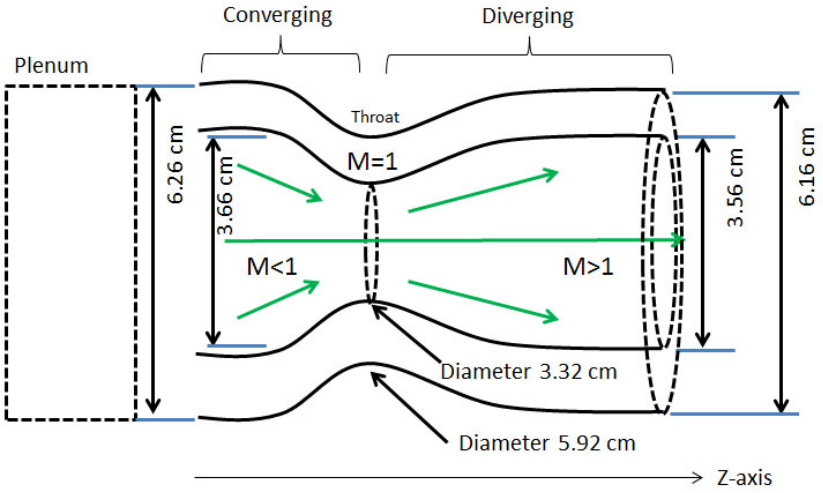

Figure 2.2: Cartoon cross-section of CD-nozzle illustrates the flow of gas from a high pressure chamber, through the throat and nozzle outlet. Mach number is labeled in corresponding sections. Green arrows represent the flow of gas.

pass through a section of minimum area. For a CD nozzle this minimum area is referred to as the throat. Conservation of mass tells us that if the mass flow rate is constant and the cross sectional area decreases the velocity must increase. At the throat where the cross sectional area is a minimum, the gas velocity becomes sonic ($M = 1$). As the nozzle cross sectional area increases, the gas flow expands and increases to supersonic velocities, i.e. Mach number > 1.0.Generally this is referred to as choked flow, which is similar to pinching a water hose and watching the water velocity increase.

2.1.2 Operation

The gas puff is activated by an electro-magnetically driven valve with a rise time on the order of hundreds microseconds. The gas puff valve consists of a magnetic coil, a hammer and a poppet valve. The valve operates by diamag-

netic repulsion between the energized magnetic coil and the copper hammer. The process consists of converting the electrical energy (in the magnetic coil) to a magnetic energy (between the coil and hammer) and then to the kinetic energy of the hammer. The electrical energy supplied by a capacitor is discharged through the coil; the flowing current produces a strong magnetic field. The magnetic field induces eddy currents in the hammer that is resting on the coil. Lenz's law tells us that the ineraction between the coil and eddy currents accelerates the hammer towards the stopper plate and pushes on the poppet. The gas puff valve is shown below in figure 2.3, with the locations of key components.

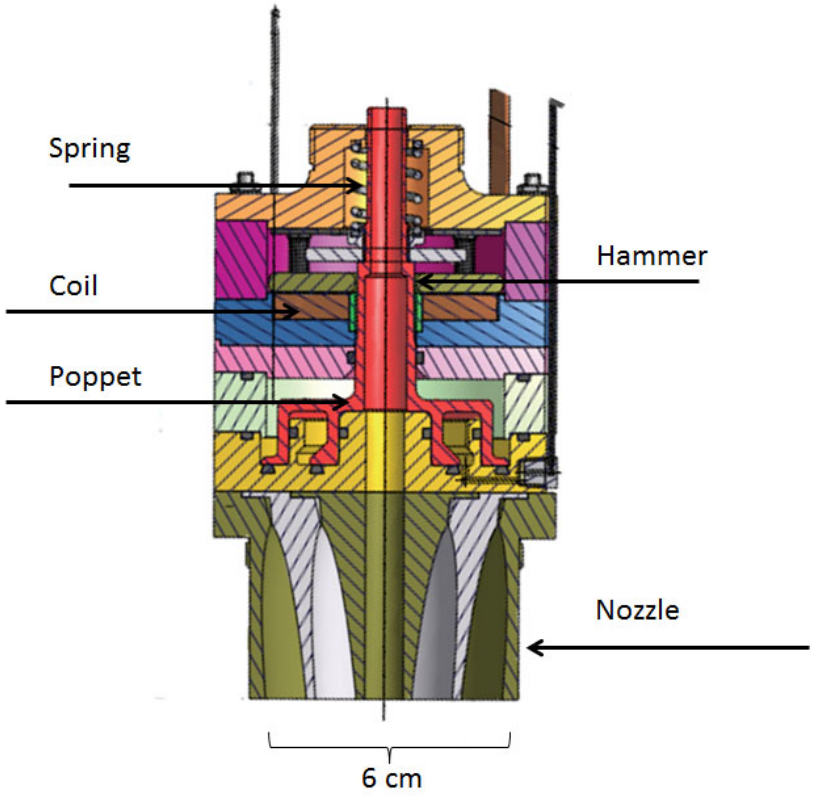

Figure 2.3: Mechanical drawing of puff valve. Key components are labeled.

The process of gas injection is described as follows. The magnetic field re-

pels the tellurium copper hammer away from the coil. When it hits the stopper plate, the force of the hammer moves the poppet which allows for gas to flow along the nicks of the inside perimeter. The aluminum 6061T6 poppet has two sealing surfaces an inner disk and outer coaxial cup. The outer cup serves as a boundary between the inner and outer gas plenums. The seal prevents any gas from the inner plenum to leak into the outer plenum whether the valve is open or closed. The gas flows from the plenum to the low pressure outlet. A reset spring automatically reseats the hammer on the coil surface after each opening. When the hammer reseats the valve closes in a few milliseconds after it opens. This action prevents completely emptying the plenum of gas. A small amount of gas has now been ejected from the plenum into our lower pressure or vacuum environment.

2.2 Laser-induced fluorescence

2.2.1 Principle and theory

The density of the gas puff is measured by using Laser Induced Fluorescence (LIF). LIF is a spectroscopic technique that uses laser radiation to excite molecules of a chosen species. The excited species is used as tracer and mixed with the gaseous flow [12]. A short wavelength pulsed laser excites a fraction of tracer molecules in the gas to a metastable state. The molecules electron transitions to a higher excited energy state and then drops down to a lower energy state while emitting a photon. The emitted photon is at characteristic wavelength and the electron is now at a stable state. This process is called photolu-

minescence and there are two types involved depending on the electron's spin, fluorescence and phosphorescence. Figure 2.4 illustrates the two processes that can occur.

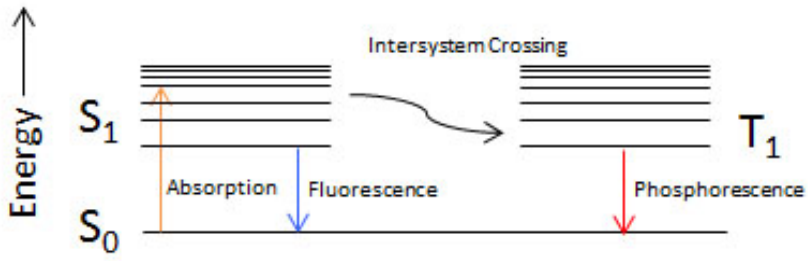

Figure 2.4: Diagram of an excited electron and the radiative decay processes that can occur. The singlet-singlet configuration of fluorescence (blue) and the triplet-singlet configuration of phosphorescence (red) are labeled.

When the excited electron has a paired spin with the higher energy state electron fluorescence occurs and is short lived. A pair of electrons in the same energy level must have opposite spins per Pauli Exclusion Principle. The electron goes from a ground singlet state to a higher singlet state before decaying by the allowed radiative process fluorescence. Fluorescence for most species lasts a few nanoseconds, for example acetone fluorescence has a lifetime of 4 ns [13]. The second type of decay process is phosphorescence which involves a dipole forbidden transition, this occurs when an excited electron undergoes intersystem crossing to a triplet-singlet configuration. The excited electron has the same spin as the electron in the triplet state and thus they are not paired. The electron is excited from the ground singlet state to a triplet state before decaying back down the ground state while emitting a photon. The transition probability is much lower and therefore has a much longer lifetime. The intensity is also weaker than fluorescence. A percentage of the tracer species transfers energy through interactions such as collisional quenching or internal conversion.

These other processes are neglected since they do not emit a photon directly.

The emitted light is typically collected with a camera as a 1-dimensional image normal to the laser beam path. The fluorescence signal collected gives a concentration of atoms in space along the beam path. For a cylindrical system such as an annular nozzle, the orientation allows for a $r - z$ or $r - \theta$ geometry. The $r - z$ system produces an axial profile of the gaseous flow at a given θ, where $r - \theta$ produces a radial profile at a given z-axis location. To expand the image to 2-dimensions a cylindrical lens is needed. Laser sheet formation is possible by the combination of spherical and cylindrical lenses to make a line focused beam. The spherical lens determines the sheet thickness and the cylindrical lens alters the sheet height [14]. The beam becomes a sheet that then excites molecules along the z-axis. Fluorescence imaging with the laser sheet is referred to as planar laser induced fluorescence (PLIF). LIF systems determine gas density profiles quickly with high signal to noise ratios along the beam path. It can be used to characterize azimuthal symmetry, flow trajectory and shell-on-shell interactions at supersonic speeds. A relative density profile is easy to obtain, but a high accurate density determination requires knowledge of the flux of photons emitted. The temperature, density and local gas composition dependence of the fluorescence yield add to the uncertainty in accurate mapping [14].

2.2.2 Acetone

Acetone ($(CH_3)_2CO$) is an organic compound that is a colorless, flammable liquid at room temperature. Acetone is an ideal tracer for laser induced fluorescence imaging of gaseous flows due to its good signal levels, low toxicity, and

accessible absorption region of 255-320 nm [14]. The absorption spectrum of acetone is a single broad band, which makes it ideal for various commercial lasers. With a maximum absorption at 275 nm, the 4^{th} harmonic of the Nd: YAG laser at 266 nm is a perfect choice. The fluorescence signal from acetone is determined by the intensity of the exciting laser beam and the number of atoms in the gas [8]. Phosphorescence emission is within the spectrum of 250-600 nm which is shifted slightly towards red. Fluorescence in the visible spectrum does not require any special camera and thus makes implementation cost effective. The maximum percentage of acetone in a mixture is determined by vapor pressure and is dependent upon temperature [16]. Acetone has a vapor pressure of 0.3 atm at room temperature. This high concentration allows excellent signal levels to be achieved [12].

CHAPTER 3

EXPERIMENTS AND SETUP

3.1 Puff system

3.1.1 Valve and nozzle

The gas shell is injected into the system from the nozzle/valve hardware mounted on top of a vacuum chamber. The gas puff is constructed by six housing stacks connected to the nozzle. Each stack is made of 60601T6 aluminum, except for the coil housing (G10), and connected with stainless steel bolts. The valve shown in figure 3.1 illustrates the gas puff and each stack location.

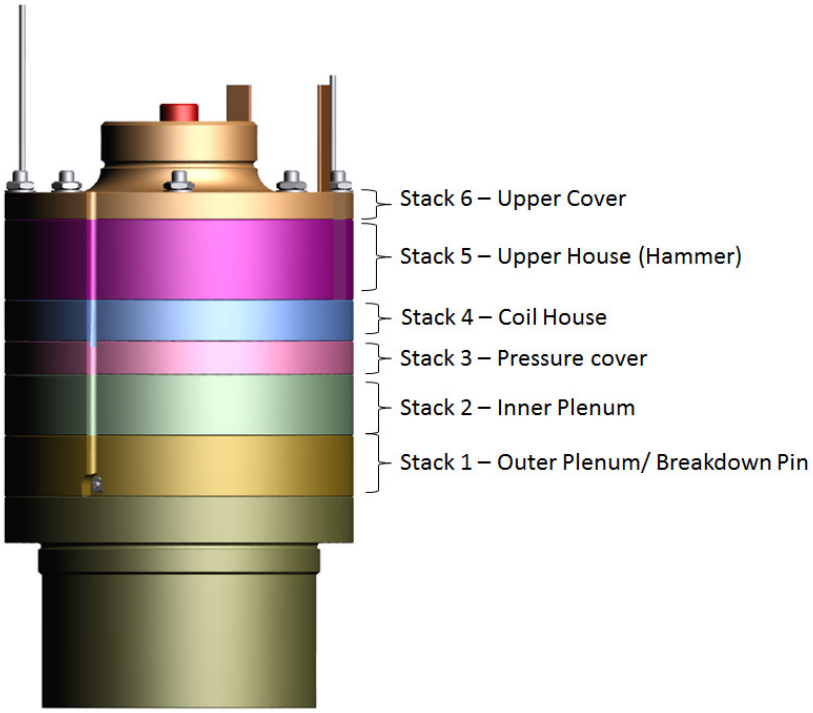

Figure 3.1: Gas puff schematic of housing stacks. Key functions of the each stack are labeled.

Each housing stack serves a different function. Stack 1 and stack 2 are used to house the outer/inner plenum. The breakdown pin is also located in stack 1. Stack 4 houses the coil. The hammer and stopper plate are located in stack 5. Stack 6 holds the housing together and contains the spring that reseats the hammer.

Opening the valve is done by discharging a 250 μF capacitor at 1 kV, resulting in 125 J. The current travels through the 31 μH magnetic coil which propels the hammer. The coil made of a copper wire with a resistance valve of 0.16 Ω. The rise time of the valve is linearly proportional to the charge voltage until it reaches a saturation level. At 800 V the valve speed is 10 m/s, with a minor increase at higher voltages [17].

Even at supersonic speeds the gas puff will diverge radially after a certain distance. The nozzles shape and thickness can help limit radially expansion [10]. If wall separations between the inner and outer nozzle are too small the two shells form one thick shell. A 1 cm separation of the two nozzles ensures that at supersonic speeds the puff remains a shell-on-shell profile [10]. The throat cross sectional area of the inner and outer nozzles is 0.32 cm^2 and 0.58 cm^2 respectively.

The gas puff requires external connections for operation and is described as follows. Two high voltage coaxial cables are connected internally to the magnetic coil and exit the side casing. Both cables have a BNC connector at the end. Creating a path for the current pulse to enter and exit without making contact with the outer conductor housing. A thinner coaxial cable is used for the breakdown pin, which will be described in section 3.1.2. Two 1/16" diameter copper pipes lead into the inner and outer plenum respectively and are fitted

with Swagelok connectors. The gas puff is mounted on a plastic radial disk of diameter 7.5″ to hold it place. An aluminum cylinder houses the gas puff in the test chamber. Four feed thru connections at the back of the cylinder are used for the gas puff's external connections.

3.1.2 Pin-trigger

A breakdown pin is inserted into stack 1, positioned between the fast valve and the nozzle outlet. The breakdown pin's main function is to monitor the flow of the gas out of the nozzle. The breakdown pin consists of one electrode that lies in the outer gas shell path at a fixed distance from the conducting wall. The pin is the inner conductor of a coaxial cable. The electrode is biased with a positive DC voltage. The ambient vacuum keeps the pin from breaking down before the flow of gas [10]. During operation the gas causes the pin to arc to the adjacent electrode, the metal surface, producing a current pulse. The pin trigger signal is illustrated in figure 3.2 below.

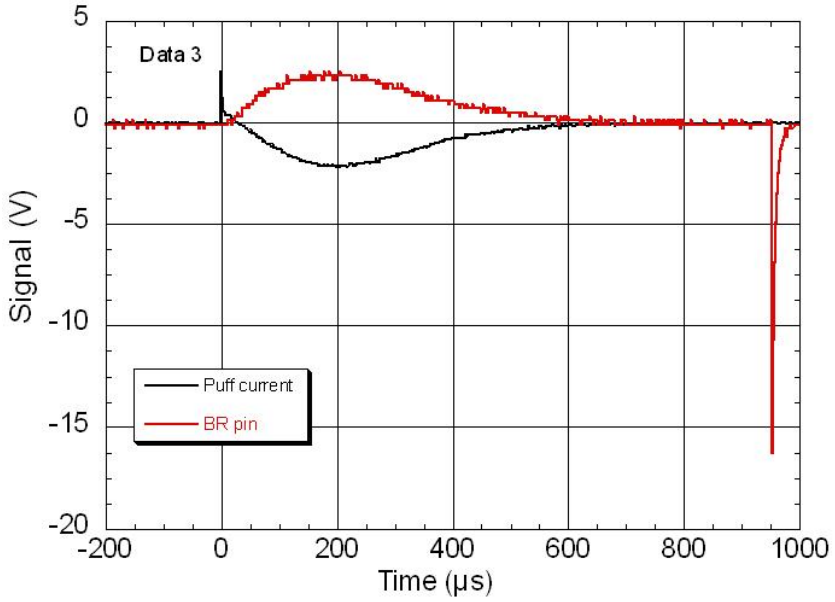

Figure 3.2: Pin trigger pulse. Black line: Driver current to the puff coil at a charge voltage of ~950V. Red line: Break-down pin signal at a bias voltage of 1kV.

As shown in figure 3.2 the driver current opens the valve and roughly a 1 ms later the breakdown pin is triggered. With repeated usage the pin becomes damaged and develops a carbon coating. It is suggested that the pin should be replaced every 100 shots. Although the pin can be biased up to 2 kV, it is suggested to use 1 kV to increase the lifetime of the pin [18]. The breakdown pin signal is referred to as the pin trigger since it will be used to activate the pulsed power machine during z-pinch experiments.

For mechanical systems there is an understood level of jitter associated with its performance, thus the pin trigger is used to reference the start of gas flow. The flow of gas is not instantaneously observed when the valve is fired. The valve opening speed is dependent on the capacitor discharge voltage. As shown in figure 3.3, the flow of gas is observed with a photodiode signal after the pin trigger.

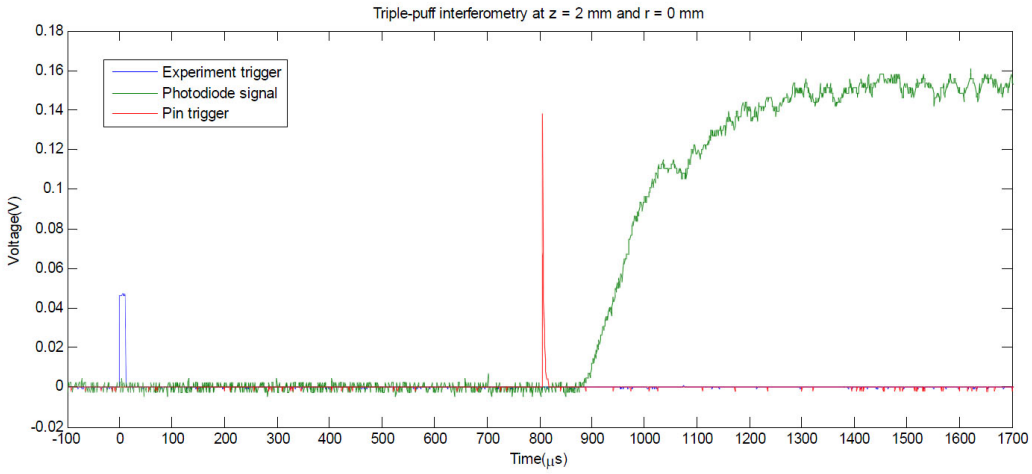

Figure 3.3: Typical timing sequence of gas puff [4]. The experiment trigger starts the sequence and fires the gas valve. 800 μs later the breakdown pin signal is observed and the photodiode signal reports the flow of gas out of the nozzle.

The Weizmann plasma group performed these measurements using 1-D interferometry on the gas puff valve. The flow of gas alters the initial phase difference of the interference pattern. The resulting fringe position shift causes the intensity to increase and is monitored by the photodiode. We see that the flow of gas ramps up to the maximum amount a few hundred microseconds after the pin trigger. Thus for triggering purposes experiments should be set during the maximum flow of gas. The maximum flow of gas is roughly 1.2 ms after the valve is fired. Typically at 1 kV discharge the pin trigger is observed at $\sim$ 940 μs. A jitter of 15 μs between shots with the same discharge voltage is observed. When different pressures are used there is a small change in the delay [4].

3.2 Control system

Operating a gas puff valve requires electrical energy and a supply of gas to inject into the test chamber. A control system is needed to activate, monitor and supply the gas puff. The system constructed at Cornell can be used for both LIF measurements and for z-pinch experiments. Figure 3.4 shows the control system mounted on a moveable rack. Except for the delay generator all other systems were constructed at Cornell.

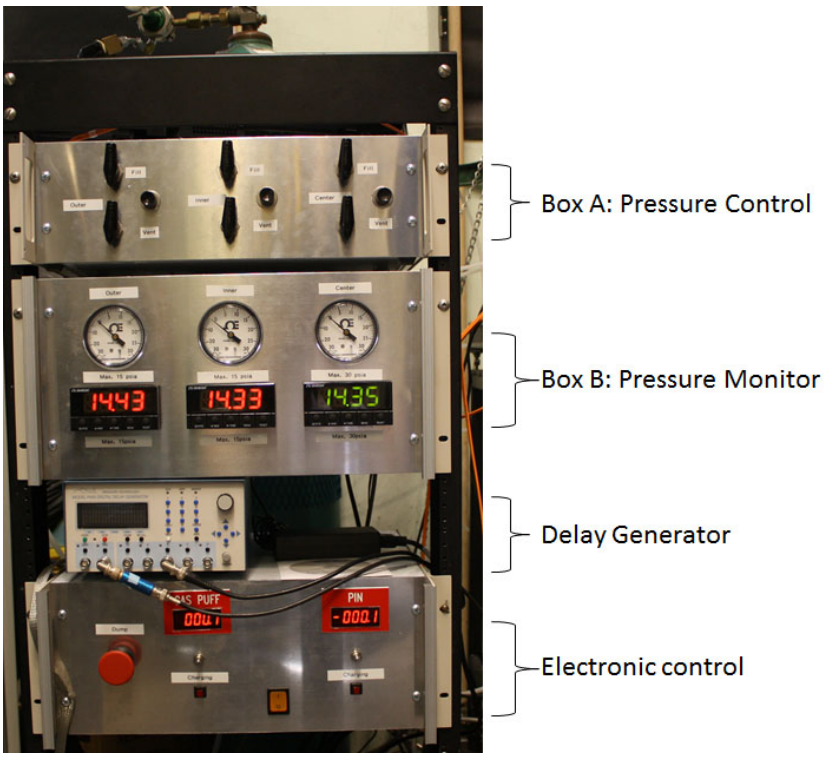

Figure 3.4: Gas puff control rack. Box A is the pressure control system. Box B is the pressure monitor system. The electronic control system is below. A P400 Highland Technology delay generator is shown.

3.2.1 Electronics

The gas puff requires high voltage for both the valve and the breakdown pin. The electronic system must meet the following requirements. Supply a HV pulse to the magnetic coil and withstand any reflection. Be able to operate multiple times a day. Charging time of capacitor must be less than five minutes, for z-pinch experiments. The systems must also be compact so it can be moved with the gas puff. The electronic system constructed is made of two circuits that supply and monitor the HV to the gas puff. An AC/DC adapter is used to supply 12V to two EMCO high voltage DC/DC converters (FS series).

The first circuit is designed as RLC circuit which sends a fast pulse to the magnetic coil. An EMCO (FS10) uses a step up transformer to convert the supplied 12V to 1 kV which charges the 250 μF capacitor. An HV SCR is connected to capacitor and acts as a switch to the magnetic coil of the gas puff. The gate of the SCR is connected to a pulse transformer to isolate the HV side from the low voltage side. When the gate of the SCR receives a 18 V pulse it closes the SCR. A Rogowski coil is attached around the HV cable to the coil, to monitor the pulse timing and length. The second circuit uses an EMCO (FS20) to step up 12 V into 1 kV. The HV side of the EMCO DC/DC supplies an open circuit voltage of 1kV to bias the pin. The pin signal is collected by an external breakdown circuit that monitors the flow of gas. The voltage of the capacitor and pin is monitored by two Murata Power Solutions digital panel monitors.

3.2.2 Pressure control

The gas puff will be used in a variety of z-pinch experiments, so the type of gas and pressure in the plenums will be adjusted accordingly. The gas density profile is determined by the pressure in the plenum, so the system must be able to adjust the pressure at any time. The pressure control system was built for three chambers with a triple gas puff nozzle in mind however it can be easily adapted to the double gas puff. The setup is designed for a pure gas and thus any mixing must be done separately. The circle diagram in figure 3.5 below illustrates the operation of the pressure system.

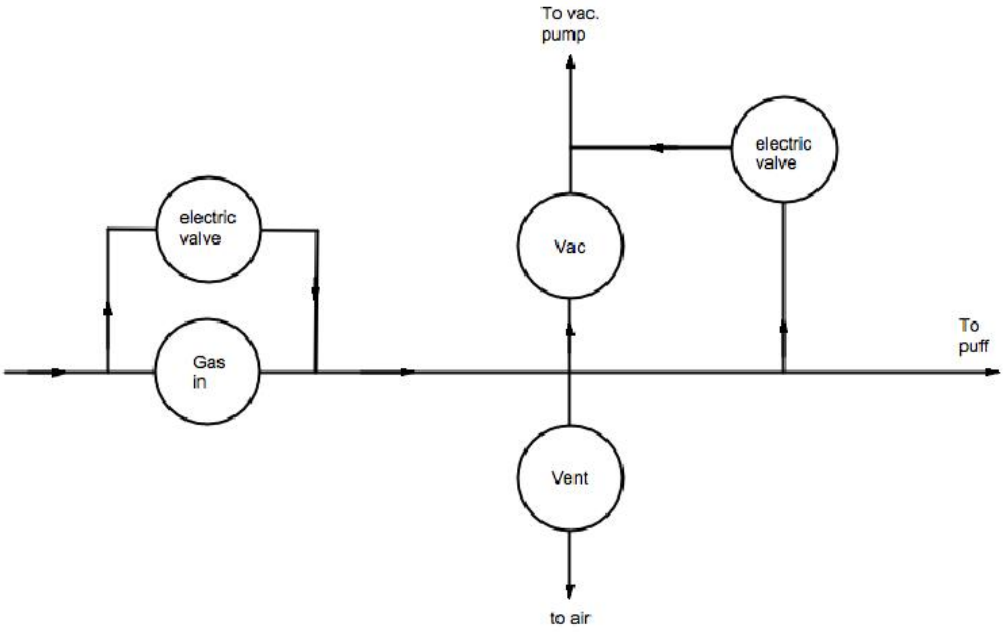

Figure 3.5: Operation of pressure system. Gas flows into the system on the left. The gas is then controlled so it can be vented to air, vacuum or lead to the puff.

The pressure system consists of two rack mounted aluminum boxes that serve two functions. Measurement of pressure in the plenums and control of pressure settings in each plenum independently. The pressure system is con-

nected with $\frac{1}{4}$"nylon tubing and brass connectors. The small pressure control box shown in figure 3.4 adjusts the pressure for each plenum. For typical gas puff experiments the gas injected is supersonic and not at atmospheric pressure. Thus adding a gas without emptying the plenums will cause poor results or damage to the valve. Gas flows from high pressure to low pressure, thus when attempting to reduce the pressure in a plenum a pump is needed. A connector on the back creates a path to the vacuum pump. For the LIF measurements it is easier to use the test chamber instead of adding another vacuum pump. The connection made to the test chamber creates a path that can lower the pressure in the plenums and allows for the test chamber to be brought up to atmosphere using the same system. A valve on the back of the box vents the system to atmosphere. Now that the plena have been emptied, the selected gas can be added to the system. Gas enters the system through three intake connectors and flows into the system and past the control valves. There are two adjustable valves for each chamber, one to fill and another to vent to vacuum. A solenoid pressure switch is installed to dump ~50% of the pressure in a chamber. The gas then leaves box A and flows into the pressure monitor box.

The larger box (B) in figure 3.4 monitors the pressure in units of pounds per square inch absolute (psia) on three digital display units. To measure the pressure a transducer is used. The transducer converts the gas pressure into analog signal. The analog signal is then read by the OMEGA DP25-RMS digital monitor and displayed in psia. After passing through the transducer the gas flows through the analog Omega PGP-25B pressure gauges. The gas then flows out of box B and into the gas puff plena.

The pressure system allows for independent control over the inner and outer

plenum. Examining the dynamics of a single puff is possible by emptying either plenum while keeping the other plenum high. Interesting shell-on-shell dynamics are revealed, as well as indications of high density regions along the z-axis.

3.2.3 Acetone mixture

For an intense fluorescence signal a certain percentage of the tracer species must be thoroughly mixed with a pure gas. Mixing acetone with a pure gas is done separately from the pressure control system. The mixture is composed of roughly 5% acetone and 95% neon gas. The acetone-neon mixture ratio is set by the pressure of the incoming neon gas. The acetone mixer was constructed at Cornell. The mixer and its corresponding schematic are shown below in figure 3.6.

The acetone container has an observation port to monitor the level of acetone inside. The mixture is created by evaporation. Acetone vapor pressure in the container is 180 torr at room temperature. The Ne gas enters the container submerged in acetone liquid. The liquid surrounds the gas creating bubbles that rise upwards. The gas evaporates towards the exit at the top of container. The rate of bubbling is determined by the pressure differences and flow rates. A micro valve controls the pressure outlet of the mixer. The rate of bubbling is observed visually by the observation port on the acetone container. Proper mixing usually occurs at the rate of 1 bubble per second [18]. When the rate of bubbling occurs too quickly a clustering effect can occur. Clustering causes nonuniform fluorescence signals and bunching around the nozzle. The gas out-

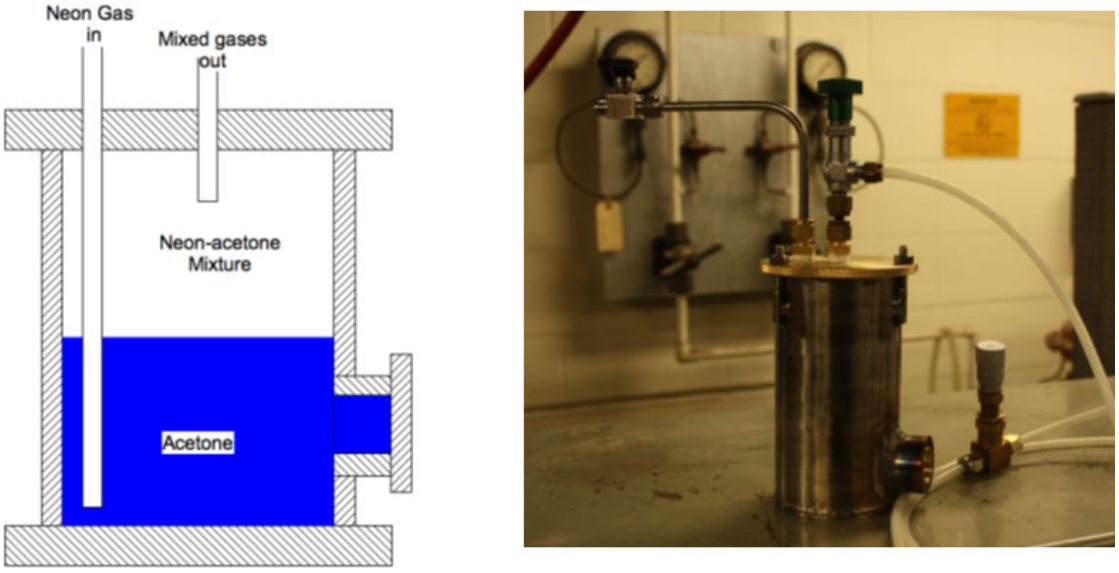

Figure 3.6: (Left) Acetone container schematic. The neon gas enters through the tube on the left. The mixed gases leave through the tube on the right. (Right) Acetone container with micro valve.

let of the mixer feeds into the pressure control system. Neon was chosen for the LIF measurements since it will be the same gas used in COBRA z-pinch experiments. The suggested pressure setting is 25 psig for the inlet of the mix-can.

3.3 LIF system

3.3.1 Vacuum chamber

The aluminum test chamber houses the gas puff valve system. The physical test chamber and corresponding schematic are shown below in figure 3.7.

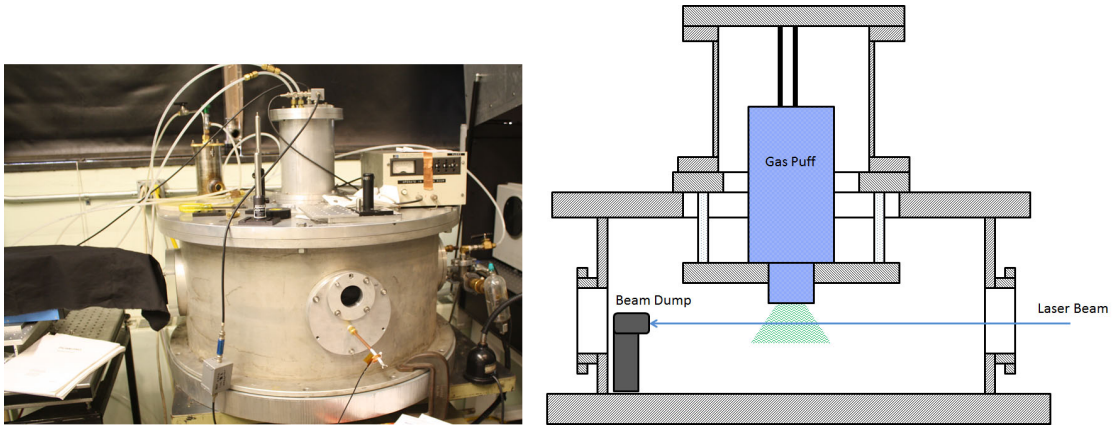

Figure 3.7: (Left) Test Chamber. (Right) Schematic of test chamber with gas puff. Gas puff is mounted in the center of the chamber facing down.

The test chamber is 0.87 m in diameter and 0.38 m in height. The inside of the chamber is coated heavily with an Aerodag G (carbon) coating. The carbon coating reduces reflections that occur from the UV laser. The test chamber is fitted with four ports and a cylindrical mount on top. The cylindrical mount houses the gas puff valve at the center of the chamber. A Turbotronix NT-10 turbo pump is connected to the chamber at the back port. A roughing pump is also connected to the test chamber. The test chamber reaches 10^{-4} torr between the two pumps. The pressure is monitored by a convection gauge until the pressure drops below 10^{-3} torr and an ionization gauge (RG-81) is needed. The observation port is fitted with a 1″ thick Plexiglass window. The beam entrance is quartz window (2″ diameter) attached to an aluminum port. Quartz is used to reduce any intensity lost when laser enters the test chamber.

3.3.2 Optic system/Streak camera

The acetone is excited by a pulsed 4th harmonic Nd: YAG laser at 266 nm with a 10 ns duration beam and circular cross section 2 mm in diameter. The energy per pulse is 80 mJ and the repetition rate is 1 Hz. The UV laser beam is focused with a 2 m spherical lens. The Edmund optics spherical lens is made of fused-silica for high power use with an anti-reflection coating. Figure 3.8 shows the path of the laser beam as it leaves the laser box and enters the test chamber via the quartz window.

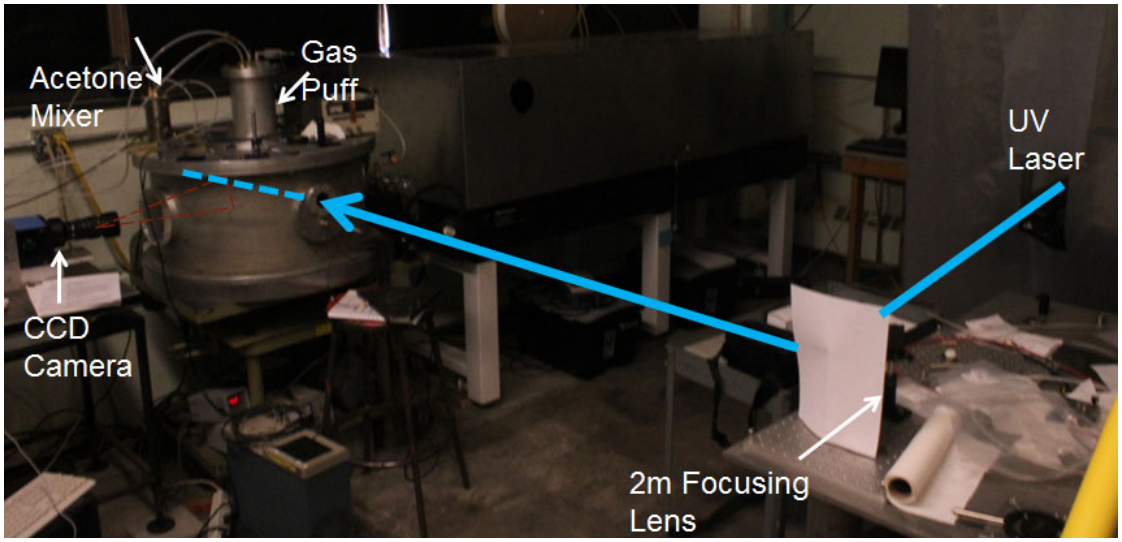

Figure 3.8: Beam path of pulsed UV laser as it enters the test chamber. A camera is placed next to the observation port. The gas puff is mounted on top of the test chamber.

As shown in figure 3.8, the beam path is illustrated by the blue line and key components are labeled. The beam is reflected off a series of UV silica mirrors before being focused by the 2 m spherical lens. LIF imaging resolution is not only determined by the camera optics but also the laser beam optics [13]. The thinner the focused laser beam is the higher the resolution. A CCD camera

is also shown next to the observation window. The beam bisects the nozzle down the center. The path of the beam creates four regions of interest from the concentric nozzles. An illustration of the beam along the nozzle is shown in figure 3.9.

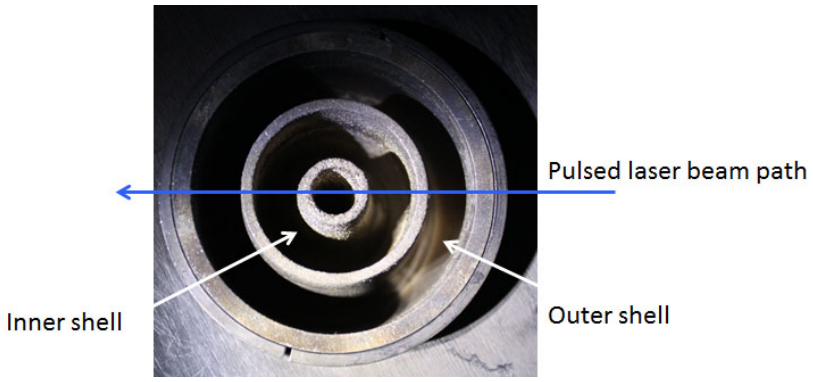

Figure 3.9: Gas puff nozzle. Inner and outer nozzles are shown. The pulsed laser beam path is indicated with a blue arrow.

The beam passes along the inner shell and outer shell twice. If the gas shell is uniform then the corresponding regions should be symmetric about the center. It is then expected that the shape and mass of the shell be similar for both regions of the same shell. For an ideal gas at supersonic speeds there is limited expansion in the radial direction so we expect to see the greatest quantity of gas along the shell regions.

The optical system can be adjusted for PLIF measurements by adding a cylindrical lens. Cylindrical lenses are commonly used in beam shaping by expanding the light in one axis. When the laser beam hits a cylindrical plano-concave lens the beam expands from a virtual source placed a distance f behind the lens, where f is the focal length of the lens. At a fixed distance from the lens there will be a line with a thickness of 2r, where r is the radius of laser beam. The spherical lens is still needed to obtain the necessary thickness of the sheet

[19]. The result is a laser sheet of finite height along the same beam path. A UV silica-fused cylindrical lens from Edmund optics was placed in the beam path before the spherical focusing lens.

The low yield of acetone fluorescence requires the camera to be as efficient as possible. The experiments conducted at Cornell used two different optical streak cameras for collecting LIF signals. A streak camera measures the variation of light intensity in time and space. The 1st streak camera is a Hamamatsu streak camera C7700 with a scientific CCD (C4742-98) attached. The recorded image is then converted to a digital signal and processed with Hamamatsus pre-packed imaging software. The magnification through the streak camera is 1:1. The 2nd camera system is a Hamamatsu streak camera C2830 that projects the streak image out of the back of the camera. A 50 mm lens is attached to the back of the streak camera and focuses the image onto a Canon Rebel T2i CCD camera. Canon ETI software is used to record any images. Images are stored as tiff files. The magnification of 2nd streak camera is 1:1.5.

The streak camera faces the observation window of the test chamber perpendicular to the beam path. The LIF signal is focused by a 55 mm lens before entering the streak camera slit. The demagnification of image into the streak slit is 6.4. The streak camera has a spectral range of 200 nm to 850 nm. The streak camera produces an image of intensity in the form of time vs. position. The width of the image is 1-dimensional variation in space, for our case the radial direction of the nozzle. The usable width of the streak camera slit is 15 mm. The length of the image shows the time variation of the signal determined by the streak sweep.

Both streak cameras operate using the same principles as described by the

operator manual and summarized below [20]. Incident light upon the slit is focused with a 35 mm lens before being projected onto the photocathode. Photons bombard the photocathode which produce electrons via the photoelectric effect. The electrons are accelerated in a cathode ray tube and pass through a pair of electrodes. A sweep circuit applies high voltage to the electrodes for a pre-determined time frame. The resulting electric field deflects the electrons down the tube. This is a time-varying deflection that sweeps the electrons onto a micro-channel plate (MCP). The electrons that arrive first are swept to top of the MCP and those that follow are deflected underneath in succession. The earlier electrons see a higher electric field than the later ones. The electrons are multiplied several thousands of time before reaching the phosphor screen. The phosphor screen converts the multiplied electrons back into photons. The optical image from the phosphor screen now gives a time profile along the length of the image. The width of the image saves the spatial information. The streak image is projected onto a CCD camera for recording. The acetone absorption spectrum does not overlap with its emission spectrum so there is no need for tuning or filtering.

3.3.3 Triggering sequence

A triggering sequence is required to operate the gas puff and record LIF signals. Operation and control of the triggering sequence is described in this section. A mechanical system with moving parts can only move so fast. It takes time for the valve to open and gas to flow. Thus there is an expected level of jitter associated with its operation on the order of microseconds. As shown figure 3.3 the flow of gas plateaus after 1.2 ms from the firing trigger. A triggering

sequence is developed to fire the laser after 1.58 ms so if the valve opens early or late the laser still excites during a high gas flow time. It is important to trigger z-pinch experiments off the breakdown pin signal since it ensures the flow of gas, however for LIF experiments the test chamber is not damaged if there is no gas. Thus the pin trigger doesn't activate the laser system but is simply used as reference for understanding the jitter of the valve. A Tektronix oscilloscope is used to monitor the triggering sequence for the gas puff. A photodiode is placed up against the quartz window to register the pulsed UV laser. The gas puff triggering sequence started by the laser output pulse (6V) is illustrated below in figure 3.10.

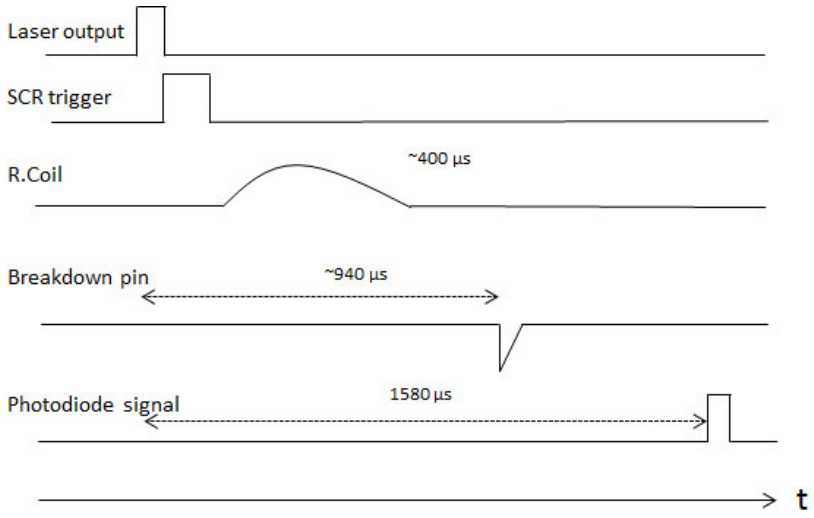

Figure 3.10: The laser output pulse starts the sequence at t=0 and triggers the delay generator. The R.coil monitors the pulse length of the firing pulse. The breakdown pin is triggered at the flow of gas and the photodiode signal registers the UV laser pulse.

The laser output pulse triggers a P400 delay generator which sends an 18 V pulse to the gate of the SCR. The SCR closes and allows the capacitor to discharge through the coil. The pulse is recorded by a Rogowski coil and monitored for timing. Roughly 940 μs later gas flows through the outer plenum and

the breakdown pin is recorded. The photodiode signal records the UV laser beam entering the test chamber at 1.58 ms.

The streak camera requires two triggers, one for the gate and another to start the sweep. There is a delay associated with the gate and start of the sweep. For a 200 μs streak sweep the sweep trigger must be sent 240 μs before the event, including the 10 μs it takes to start the sweep. The gate requires 60 ns to open, however in our system this short of a time frame can be neglected. The gate trigger opens the gate for 100 μs before closing, if the sweep trigger is started anywhere in this time then the sweep starts and the gate remains open until the end of the sweep. The triggering sequence is started with laser output pulse. The streak trigger sequence is shown below in figure 3.11.

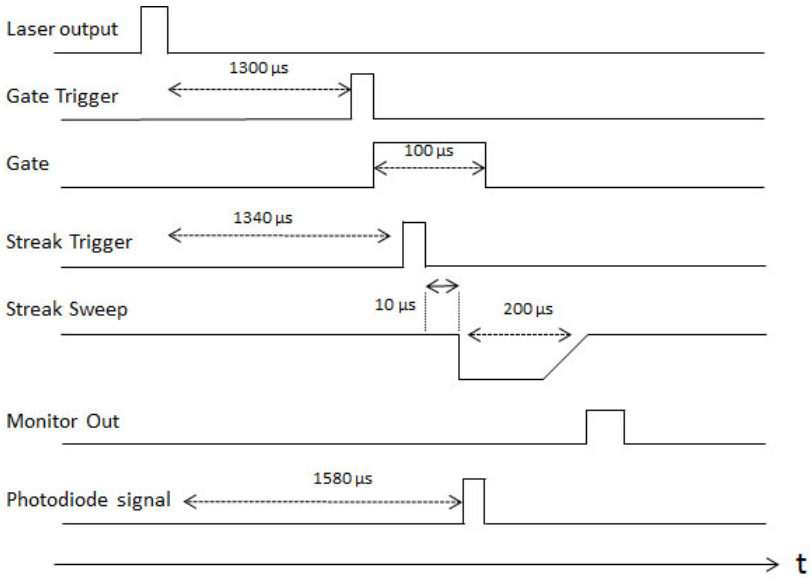

Figure 3.11: The laser output pulse starts the sequence at t=0 and triggers the delay generator. The delay generator sends a pulse to the gate at 1.3 ms. A second pulse is sent to the streak trigger at 1.34 ms. The streak is started and the monitor out pulse announces the end of the streak. The photodiode signal confirms the arrival of the UV laser.

As shown in figure 3.11, the laser output pulse starts the sequence and triggers the delay generator. The delay generator waits 1.3 ms before sending a pulse to the gate; the gate remains open for 40 μs before the delay generator sends a pulse to the sweep trigger. The streak trigger is started 240 μs before the pulsed laser beam and photodiode is observed during the streak. The sweep starts at 1.49 ms and ends at 1.69 ms. The long exposure ensures that the LIF signal is captured. The streak camera sends a monitor out signal when the sweep is completed. The monitor out signal is observed at 1.70 ms. The triggering sequence can be adjusted for a shorter sweep if needed.

CHAPTER 4

RESULTS

4.1 Imaging

4.1.1 Streak images

The LIF images are examined, analyzed and evaluated to determine the relative density profile of the gas puff. The first set of images was taken with the streak camera (Hamamatsu C7700) injunction with a high sensitivity CCD camera (Hamamatsu C4742-98). The second set of images was taken with a Hamamatsu C2830 streak camera with the low-end Canon Rebel T2i CCD camera. The images are saved as 16-bit 1280x1024 tiff files. The spatial resolution of the image is roughly 0.05 mm. Each streak camera has captured its own images that are examined and described below. The drastic difference between the two streak/camera systems is due to the two different CCD cameras used to record the images. Typical raw LIF images taken with the C7700 streak camera along with gas puff nozzle are shown in figure 4.1.

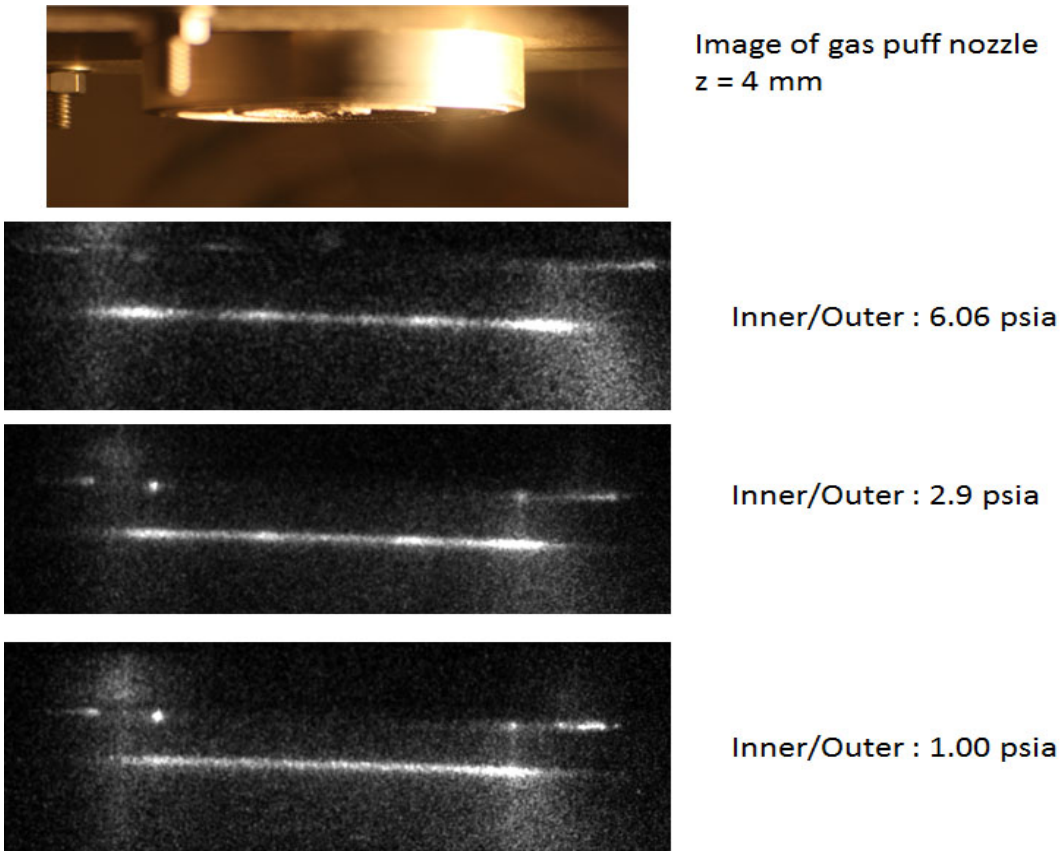

Figure 4.1: Top: image of the nozzle; Lower: Three raw LIF images obtained from Hamamatsu C7700 streak camera. The beam path is 4 mm below the nozzle. The pressure in each plenum is listed next to the image. Streak sweep is 200 μs for all images.

The pulsed UV laser beam passes 4 mm (z = 4 mm) below the nozzle. Figure 4.1 shows three LIF images at pressures of 6.06, 2.90 and 1.00 psia. The Hamamatsu software filters out the green color produced by the phosphor screen replacing it with a black and white contrast. The gain of the cameras intensity is adjusted via the software and the streak sweep is set at 200 μs. The gas puff fluorescence signal is observed as a thin line underneath the nozzle. Scattered light off the nozzle is visible in each image especially at the nozzle edges. It should be noted that the scattered light from the nozzle is reduced the further

away the beam path is from the nozzle. At higher pressures the fluorescence signal is more intense in the nozzle shell regions. At the lower pressure puff, the fluorescence intensity is more uniform along the signal.

The calibration image, which will be discussed in section 4.1.3, is the fluorescence images obtained by static filling of the test chamber, where the test chamber is closed off from the vacuum pump and filled with ~1 torr of the neon/acetone mixture. The pulsed UV laser beam is fired into the test chamber and excites the acetone in the static mixture along the beam path. The gas puff is not triggered. The static fill fluorescence image is displayed below in figure 4.2.

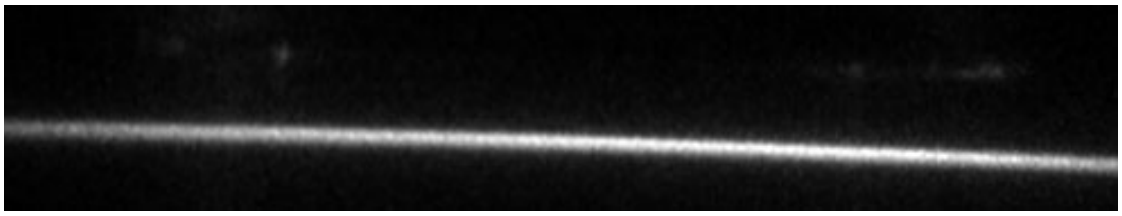

Figure 4.2: Calibration image. Fluorescence signal at 1 torr Ne/acetone mixture. No gas puff. Streak sweep is 200 μs.

The calibration image is an intense fluorescence signal that spans a width of 8 cm across the image. Scattered light from the nozzle is less visible due to the high contrast between the scattering and the brighter fluorescence beam signal. The calibration intensity is a reference for the pulsed UV laser beam shape and energy. Focusing of the laser beam is much easier to perform on the static fill case. Now that the raw LIF images for both the gas puff and static fill fluorescence are collected the data can be interpreted and a relative density derived.

The second group of streak images are taken with the Hamamatsu C2830

streak camera and recorded with the non-scientific Canon CCD. The pressure in each plenum was controlled independently. LIF measurements in various pressure combinations were examined. To fully investigate the distribution profile of the gas puff in each shell three cases were examined. These are Case A: inner shell only (no gas in the outer nozzle plenum); Case B: outer shell only; and Case C: the typical pressure setting used on COBRA, i.e. 2.45 psia in the inner nozzle plenum and 0.59 psia in the outer). The nozzle plenums were filled with neon/acetone mixture and a series of shots from high to low pressure in sequence were performed. Previous work has shown that the densities from the two gas shells are not independent of each other but shell-on-shell interactions alter the shape of overall puff density profile [6]. In case B, the outer plenum is filled at high pressure and inner plenum is emptied before a shot. This technique is not ideal since it increases the net force applied by the gas on the poppet [10]. A better technique would be to place an O-ring seal in the inner nozzle and a static fill in the inner plenum. The procedure is then switched to the outer plenum and the inner shell is examined. The original objective is to characterize the distribution profile at the pressure settings that will be used on COBRA. The pre-determined COBRA pressure settings of 0.59/2.45 psia in the outer/inner plenum were examined. Figure 4.3 is a collection of raw fluorescence images from the second streak setup, where the signal to noise ratio is poor.

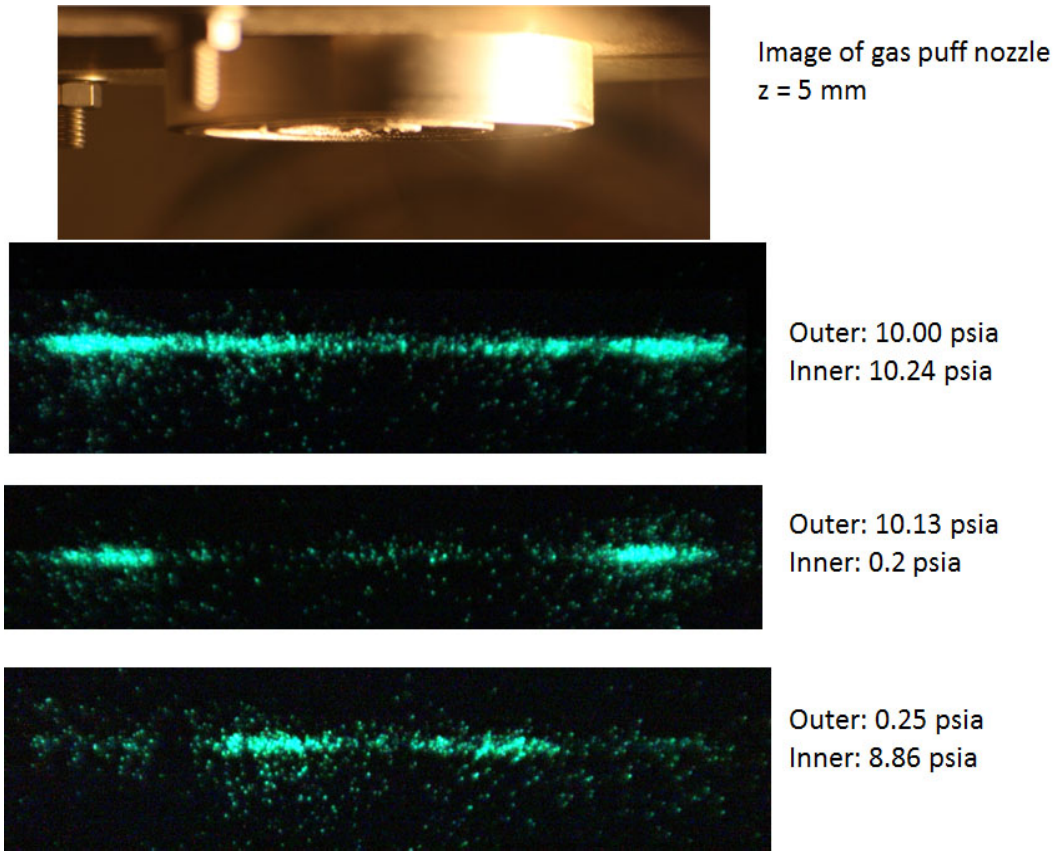

Figure 4.3: Raw LIF images from C2830 camera. The beam path is 5 mm below the nozzle. The pressure in each plenum is listed next to the image.Streak sweep is 200 μs for all images.

Three LIF images of the gas puff are shown in figure 4.3, the first when the pressure in each plenum is high, the outer shell at high pressure, and finally the inner shell at high pressure. The green color in the images is the phosphor screen of the streak camera captured by the Canon color CCD camera. However the images are of poor quality as the signal levels in lower pressure regions are too low and of inferior resolution. The gain of the system is controlled by the streak camera itself and Canon camera (ETI) captures the streak image. The lower density regions of gas puff are visible as scattered flecks in the beam path. The symmetry of the gas puff shell is still apparent but the intensity is drasti-

cally skewed. This is most noticeable when comparing the outer shell regions to each other. At high pressures distinguishing between the inner and outer shell regions is apparent but resolution in low density regions is poor. The gain of the camera is not sufficient to produce high quality images particularly in low density regions. Using this streak camera, we have captured a new calibration image for reference. The calibration image also helps illustrate the point of insufficient gain along the laser beam path as shown below in figure 4.4.

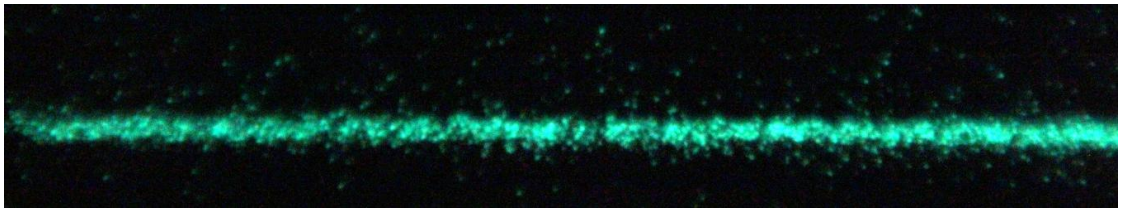

Figure 4.4: Calibration image. Fluorescence signal at 1 torr Ne/acetone mixture. No gas puff. Streak sweep is 200 μs.

Again, in the calibration image the chamber is flooded with the same neon/acetone mixture at a pressure of 1 torr. There is a drastic difference between the calibration images captured by the two streak cameras (see figure 4.2 and figure 4.4). As shown in figure 4.4, the fluorescence signal appears as bright bunches littered with dark gaps. The reduced gain of the system is the cause of the dark spots along the signal and illustrates the limitation of this optical system. These gaps in the laser beam path become a significant problem in determining the density of the gas as described in section 4.1.3.

4.1.2 PLIF images

A cylindrical lens was added to the optical system so that the laser beam was expanded in z-axis in the PLIF measurements. The laser sheet has a height of 10 mm that excites a region of z=1-11 mm below the nozzle. PLIF measurements were taken with C7700 streak camera. An example PLIF image is shown in figure 4.5.

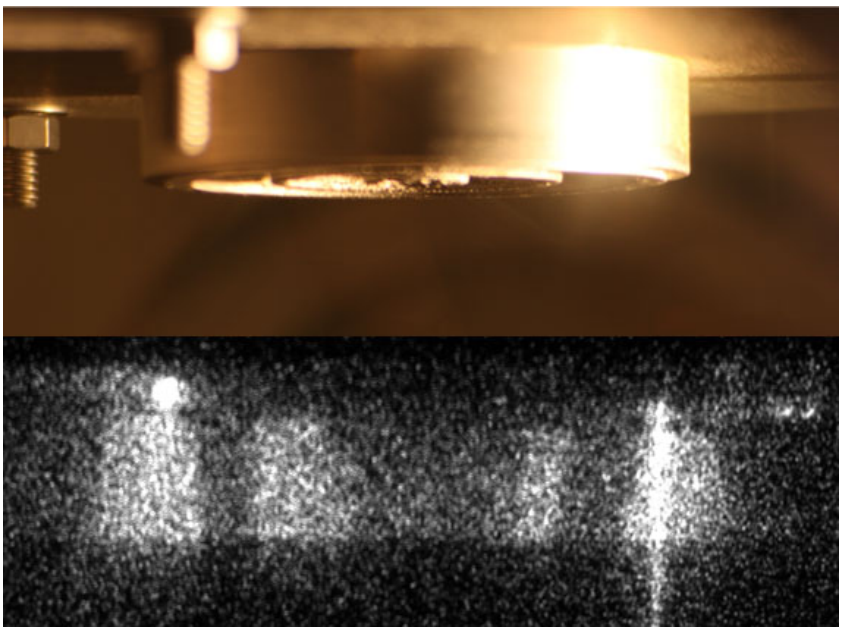

Figure 4.5: PLIF image. The gas puff nozzle is pictured above the collected PLIF image. The laser sheet height is 10 mm. The pressure in the inner and outer plenum is 4.6 psia.

As shown in figure 4.5, the PLIF image displays a 2-dimensional concentration map of the gas puff. The image reveals the structure of each shell along the z-axis. The gas is clearly collimated along the z-axis which suggests supersonic speeds. The puff converges toward the z-axis due to the inward radial motion. The scatted light from the nozzle tip is increased in the PLIF images.

4.1.3 IDL software

The LIF images were processed with an imaging software package written in Interactive Data Language (IDL). IDL is commonly used for scientific programming, image and data analysis. In the image analysis, we use a 1-D array-oriented operation that examines each vertical line in the image for the peak intensity due to the fluorescence. The density can then be calculated from this intensity as compared with those in the calibration image. The IDL program requires three images to determine the density in the fluorescence images. The three images are a gas puff fluorescence image, a background image, and a calibration image. The gas puff fluorescence image is referred to as fluorescence (FL). The background image (Bk) is the noise associated with scattered light from pulsed laser beam in the absence of the gas puff, where the images are captured when the laser is fired into vacuum ($< 10^{-4}$ torr) without the gas puff. Any light that is captured is the result of scattered light from nozzle or chamber walls. The calibration image (Cal) is a picture of the laser fluorescence when the vacuum chamber was filled with a static pressure (~1 torr) of the neon/acetone mixture gas. The Cal image shows a uniform fluorescence signal along the laser beam path since the entire test chamber contains the Ne/acetone mixture. Each image is converted into a float and constructed as a 1-D array. Then the program performs the following operation as shown in equation 4.1.

$$\frac{FL - Bk}{Cal - Bk} \tag{4.1}$$

The program creates a series of rows which are summed to obtain the signal trace as a function of the radial position along the nozzle. Then the background trace (base line) is subtracted from both the fluorescence image and the calibra-

tion image to remove scattered light. The normalized intensity is determined by the ratio of the base line corrected images. The ratio normalizes the fluorescence signal to the excitation laser energy. All three images are taken during the same set of experiments. The optics remains the same between the shots so that any image variations along the beam path are compensated for. The same Ne/acetone mixture is used in both the static fill and gas puff case so that the absolute value of the acetone mole fraction does not need to be known for this measurement [21]. The program then outputs the intensity over the radial position as a excel file. Figure 4.6 is an example of the analyzed LIF data from a fluorescence image aligned along the radial axis.

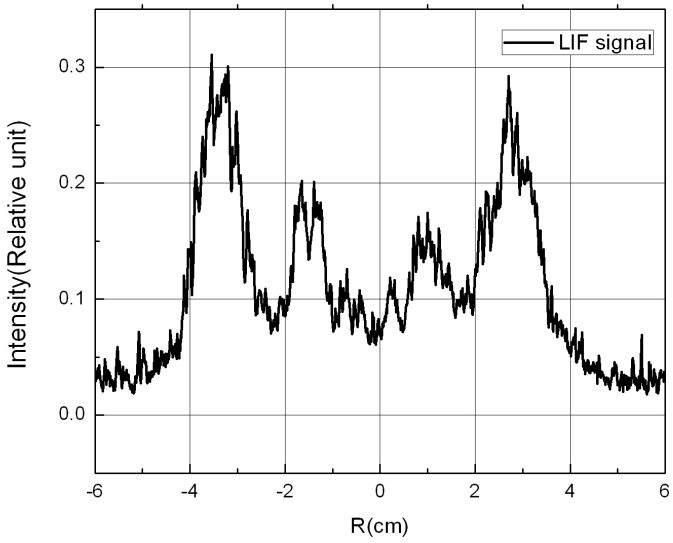

Figure 4.6: Relative intensity plot from IDL output. Y axis is the unitless relative intensity. X axis is the radial position in cm. Plenum pressure is 4.3 psia.

It is straightforward to derive the density of the gas puff from the IDL output data. The IDL output is the normalized fluorescence intensity to the laser energy corresponding to the radial position. The linear factor between the flu-

orescence intensity and the gas density is obtained if we know the gas pressure and assume ideal gas dependence of density on pressure and temperature [6]. Multiplying the ratio of normalized fluorescence intensity to those obtained in the known static fill density of the calibration image gives a relative gas puff density. At seas level and a temperature of 20 C, the density of neon is 2.68e19 #/cm^3 at 760 torr. The density of neon at 1 torr static fill is 2.68e19/760 = 3.54e16 #/cm^3. The assumption is that the mixture is at the same relative density as pure neon gas. Equation 4.2 shows the IDL output multiplied by the density at the calibration image.

$$\frac{FL - Bk}{Cal - Bk} * Density(@Cal) \tag{4.2}$$

The estimated density is then converted into g/cm^3 by multiplying the molecular mass number of neon and then dividing by Avogadros number. Typically densities are on the order of micrograms per cubic centimeter.

4.2 Relative density plots

4.2.1 LIF results

Now that a method for determining a relative density from LIF images has been established, various gas puff pressures are examined. All relative density plots come from the LIF images produced by the C7700 streak camera. An investigation of the C2830 streak camera LIF images is conducted along with its inability to produce reliable plots due to the poor signal to noise ratios in the images. Figure 4.7 is a relative density plot with associated uncertainties when both the

inner and outer plenum pressures are at 4.3 psia.

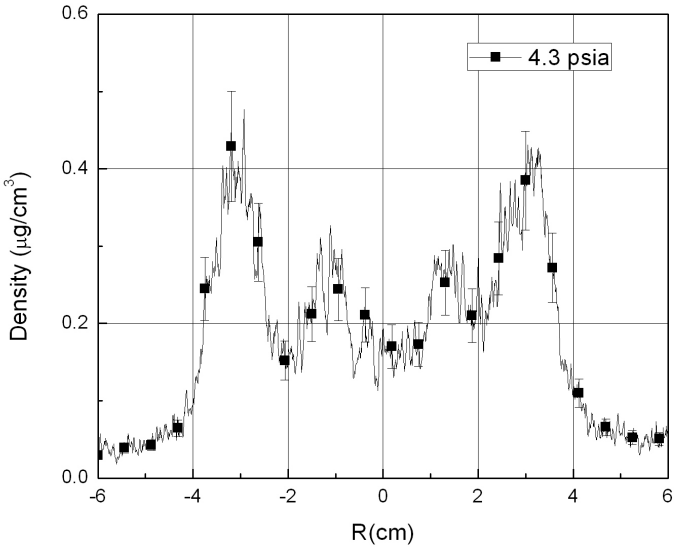

Figure 4.7: Relative density plot. Y axis is density in $\mu g/cm^3$. X axis is the radial position in cm. Plenum pressure is 4.3 psia.

The relative density plot in figure 4.7 shows the density over the radius of the nozzle and its associated uncertainty. The uncertainty in the plot is determined in the next error analysis section 4.3. The inner gas shell is located at ±(0.7-1.8) cm and the outer gas shell is located at ±(2-3) cm. Four distinct peaks along the puff diameter represent the two gas shells. The high radial spatial resolution of the LIF approach allows these narrow density features to be observed. The two peaks closest to the center make up the inner shell. The two peaks at the edge of nozzle are the outer shell. The two corresponding peaks are more or less the same. The density and symmetry between each shell are clear. Density peaks are observed at r = ±1 cm, ±3 cm. The shapes of the peaks are close to Gaussian and the peak density is roughly 1e16 $\#/cm^3$. The low density region in the center of the nozzle is 4e15 $\#/cm^3$.

A series of gas puff shots were performed in sequence with a starting plenum pressure of 14 psia and ending at 0.15 psia. The gas puff valve was fired every 5 minutes without replenishing the plenums. This was done to observe any changes in the gas flow from the valve. The data reveals a noticeable transition from laminar to non-equilibrium gas flow. The density of a high pressure laminar flow is illustrated in figure 4.8, along with a low pressure density plot for comparison.

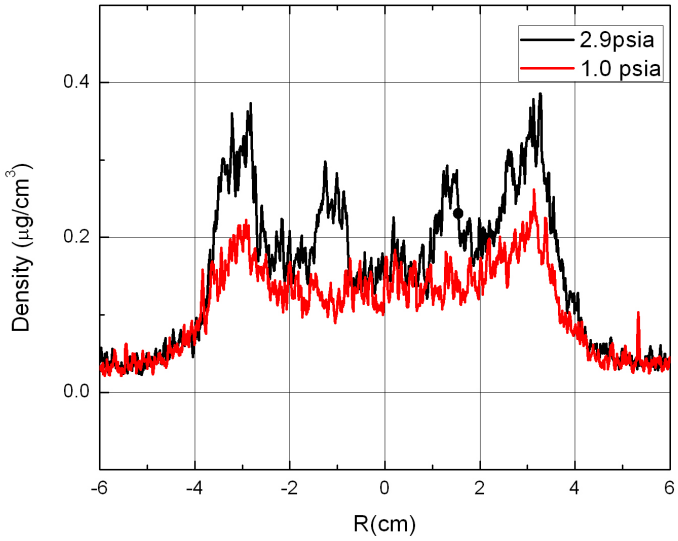

Figure 4.8: Relative density plot. Y axis is density in $\mu g/cm^3$. X axis is the radial position in cm. The black line is the puff density at 2.9 psia. The red line is the puff density at 1.0 psia.

At low plenum gas pressures the profile is more or less flatten and lacks distinct inner shell peaks. The outer shell peaks at r = ±3 cm are still noticeable at a reduced density. The transition from laminar flow occurs when the pressure in each plenum is below ~2.2 psia. The lack of collimation and uniform gas distribution in the inner shell shows that the gas has expanded in the radial direction. The gas expansion results in shell-on-shell collisions and lower peak

intensities. The non-equilibrium flow suggests the gas velocity is no longer supersonic. The peak density is roughly 40%-50% greater in the higher pressure puff. Upon visual comparison of LIF signals in figure 4.1, the higher pressure LIF signal is brighter in the shell regions. The more intense regions indicate a higher gas density along with collimation in the gas jet. The 1.0 psia LIF signal of figure 4.1 shows a more uniform intensity along the beam path.

As discussed previously in the imaging section 4.1.1, the LIF images captured by the Canon CCD have poor signal to noise ratio due to the lack of the necessary CCD gain to determine a relative density. The IDL program for determining the intensity output produces unreliable results. The main cause of this is the low signal level to properly normalize the calibration image with the fluorescence image. The calibration image shown in figure 4.4 is littered with dark spots that when converted to floating numbers are set to zero. Attempts to alter the code by adding a constant or skipping over the zeroes results in faulty data. However taking the raw fluorescence image and with no filtering it is possible to produce an intensity plot. An example intensity plot is shown below in figure 4.9.

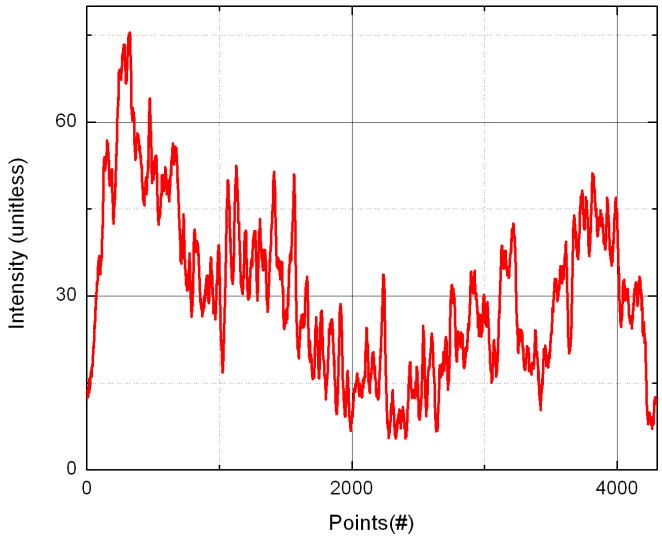

Figure 4.9: Intensity plot of raw LIF image from C2830 streak camera. Y axis is the intensity. The data points along the spatial direction in the image make up the x axis. Pressure of outer plenum is 10.00 psia and the inner plenum is 10.24 psia.

The intensity plot illustrates the four peaks however the symmetry and shape of each peak are distorted. Any scattered light or background noise is added to the intensity plot resulting in large uncertainties. The noise clearly boosts the intensity in the first outer shell peak. The inner shell lacks distinct peaks. The low gain of system and the limited spatial resolution makes the C2830 streak camera a poor choice.

The plenum pressure is monitored before and after each gas puff pulse. As expected the relative pressure drop is linear when the gas injection tends to stagnate at lower pressures. The plenum pressure drops roughly 10% between each puff pulse. The stagnation region occurs at pressures below 0.20 psia where fluorescence intensity is weak and pressure gauge sensitivity is poor.

Integration along the radial component of the density is used to determine the linear mass of each gas shell. The linear mass ejected from the nozzle is highly dependent on the nozzle geometry and plenum pressure. For the fast acting valve there is an upper limit to the mass ejected from the nozzle. Six density profiles at different pressures are examined and the linear mass is found to decrease with plena pressure as shown below in figure 4.10.

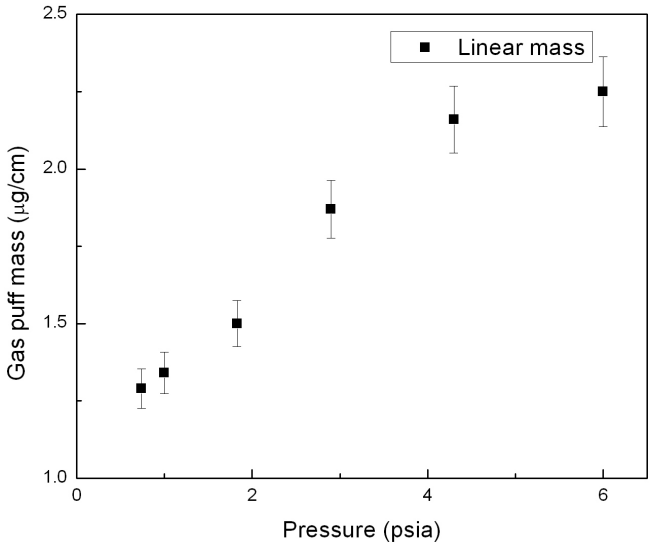

Figure 4.10: Linear mass plot. Y axis is the gas puff linear mass in μg/cm. The x axis is the pressure in psia.

The linear mass ejected from both nozzles is around a few μg/cm. The total linear mass of the double gas shells is lower than expected. For plena pressures of 4 to 6 psia the linear mass is roughly 2.5 μg/cm. Assuming that gas is pure neon and ideal then we can calculate the linear mass based upon plenum pressure. The linear mass of both the inner/outer nozzle is found to be 30 μg/cm. The estimated linear mass is an order of magnitude greater than the measured value. Further investigation in the uncertainty of the LIF system and calibration

method is needed.

A density plot of the PLIF measurement was derived using the same techniques. The plot shows the shape of the gas below the nozzle and its concentration.

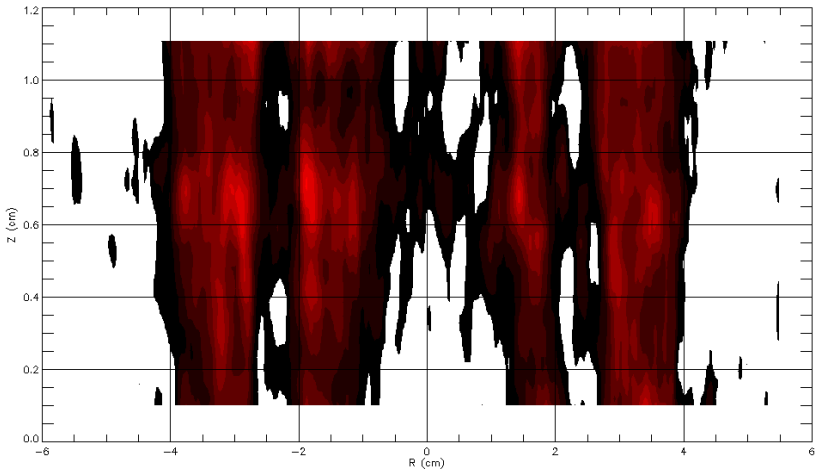

Figure 4.11: Concentration mapping of gas density below the nozzle. The laser sheet height is 10 mm and the streak is 200μs. The pressure in the plenum is 4.6 psia.

4.3 Error analysis

The LIF measurement uncertainty is 16.65%, which consists of 2.55% systematic and 14.10% random uncertainties. The systematic uncertainty is the result of image magnification and pressure gauge uncertainty. The random uncertainties are caused by shot-to-shot variation and uncertainty in the static fill fluorescence intensity. Error analysis was only performed on the images produced by the C7700 streak camera due to the inability to ascertain a final relative density for the C2830 streak camera.

The calibration of the image size is ascertained by ratio of pixels to the physical dimensions of the gas puff nozzle. The ratio is set by measuring the diameter of the nozzle in the image and then comparing to the physical dimension of the nozzle. The uncertainty is at least two pixels on each edge of the nozzle. The 6 cm nozzle is found to be 1053±4 pixels long. The uncertainty in the radial position is 0.37% along the nozzle and 0.91% in the integrated line density. As long as the imaging system is unchanged there is no relative error in the magnification between the images.

Two different gauges are used to monitor the gas pressure in this study. The Omega gauges which read the gas pressure in both plenums have an uncertainty of 0.34%. The pressure in the test chamber is monitored by convection gauge. There is a 1.3% uncertainty in the pressure gauge reading. Atmospheric pressure shifts are neglected due to the stability in day to day pressure measurements.

There is an uncertainty in the static fill fluorescence intensity due to lack of baseline reference for contrasting. This uncertainty is not there in the gas puff or background images. The gas puff fluorescence intensity can be baseline subtracted at large radial positions since there is very little gas there. This cannot be done in the static fill calibration where the whole chamber is filled with the Ne/acetone mix and there is no baseline for comparison. The uncertainty is the variation between the intensity at the baseline location and the fluorescence signal. The intensity of the baseline signal is about 490 and the fluorescence signal is 6745 which gives an uncertainty of 7.3%.

The shot-to-shot variation is determined by the estimated reproducibility of the puff valve. The reproducibility of each gas puff shot is calculated from

the standard deviation of multiple calibration images. The standard deviation along the line density is 6.8%.

CHAPTER 5
DISCUSSION

The basic principles of LIF are demonstrated and the results examined. The LIF system constructed at Cornell is designed for continual operation beyond the focus of this thesis. The spatial resolution of LIF images allowed for measurement of high density peaks where the intensity increased by 40%-50%. Gas density profiles have shown gas collimation at pressures above 2.2 psia. The linear mass ejected by the gas puff is limited by the pressure of the system. If plenum pressure is too low the puff is subsonic and the density of each shell is significantly reduced. The flow velocity is assumed to decrease but the rate is unknown. A method of measuring the gas velocity should be considered.

Calculating the relative density relies of three distinctions. The mixture density is assumed to be the same as pure neon, the pressure monitored in the test chamber is absolute, and the pulsed laser beam energy has no variation. Examining the mixture ratio and its effect on the excitation intensity would require two separate mixer containers. One mixture would be created and let sit for twenty-four hours and a second mixture of the same ratio would be created right before the experiment. Differences in intensities can then be observed in the two mixtures. LIF studies have shown a correlation between temperature and fluorescence intensity. Any temperature dependence in fluorescence intensity is neglected in this study. The normalization of the fluorescence intensity to the static fill case is also assumed to be linear. Measurement of the lasers energy would be required to ascertain an absolute density. The energy of the UV pulsed laser beam is assumed to be the same for every shot which may not be the case. In cases where the laser energy varies between pulses the IDL output would

be inaccurate. Investigation into linear mass reveals lower than estimated mass ejection from the valve. The linear mass is determined by integrating the calculated density profiles along the nozzle's diameter. Assuming the mixture is pure neon and ideal gas dependence the estimated linear mass is found to be an order of magnitude higher. This may be caused by variations in the laser energy or incorrect measurement of the pressure in the test chamber.

Phosphorescence is a weak slow decaying emission from the excited acetone. In a gas puff phosphorescence decay is observed downstream from the brighter fluorescence signal. Both streak cameras are unable to capture the phosphorescence signal due its low intensity. Studying the phosphorescence signal can distinguish gas flow trajectory and be used for accurate velocity measurements. Phosphorescence measurement is an excellent way to characterize gas flow using the same principles as LIF. Investment into a camera with significant greater gain would be required.

Improvements to the control system can help reduce uncertainty and increase the lifetime of the valve. The pressure control system had continuous leak issues while connected to the solenoid vent switches. Bypassing the switches has stopped the leaks. The issue is believed to be caused by the brass fittings. It suggested that the high priced steel fittings be used if problems persist. After repeated use the digital voltage monitor has increased in measurement error. The original error of 3% has increased to 20%. The actual voltage across the capacitor has not changed and is confirmed with a Fluke multimeter. Thus the error in the digital display monitors may be a failure to protect the units from high voltage since it located in parallel with the capacitor.

The large uncertainty in LIF measurements (16.6%) is mainly due to the random error in the experiment. The systematic uncertainty of the system has been minimized. Reproducibility was improved significantly with the aid of the P400 delay generator. The original delay generator had significant jitter even on the microsecond scale. Replacing the old generator with the P400 had noticeable results in streak images and reducing the jitter in the breakdown pin. The largest source of uncertainty is the fluorescence intensity in the static fill case. For the static fill case the intensity along the line density should be uniform. Variation in the laser energy may result in weaker intensity and attribute to unknown factors. Improvement in reproducibility and fluorescence intensity should be examined for future studies.

CHAPTER 6

SUMMARY

This study has demonstrated that the density profiles of a neon gas puff load can be determined using LIF. A control system was constructed for operation of the gas puff valve in both LIF and z-pinch experiments. The system monitors the pressure in each plenum and allows for a variety of pressure settings. LIF measurements were performed in a test chamber at roughly 10^{-4} torr with a pulsed UV laser beam. The neon gas flow was seeded with an acetone tracer of roughly 5%. The acetone was excited with a 4th harmonic Nd: YAG laser at 266 nm. LIF measurements were recorded with a Hamamatsu streak camera and CCD camera. The 6 cm double puff valve was fired in repetition from high to low pressure. The gas puff is aligned in $r-z$ geometry and the focusing lens can be adjusted for measurement at different heights along the z-axis. Density peaks are observed on both sides of the nozzle. The sub-millimeter spatial resolution of 0.05 mm allowed observation of density peaks at r = ±1, ±3 cm. Peak widths are roughly ~1.0 cm and the shape of peak is close to Gaussian. The peak density is found to be roughly 1e16 #/cm^3. Lower density regions around the center of the nozzle were found to be 4e15 #/cm^3. LIF measurements can be performed with relative ease thus a large data set was collected for examination of shot-to-shot reproducibility. The usage of different pressure ratios in the gas valve plenums has shown interesting gas dynamics. At high pressures the gas flow is laminar at the observed distance of 4 mm. At low pressures the gas undergoes radial expansion and non-equilibrium flow. The narrow density peaks are reduced at lower pressures and the peak width increases. Gas injection at low pressures is nonlinear and stagnates at the limit of the value. Uncertainty in the plenum pressure is also high for pressures below 0.20 psia. The COBRA pres-

sure settings 2.45/0.59 psia inner/outer plenum is designed for more uniform density distribution between shells. COBRA operating pressure for the outer plenum is below the transition cutoff and the effects of non-equilibrium flow on the gas load should be noted. Measuring the fluorescence intensity yields high uncertainty due to random errors and poor shot-to-shot reproducibility. Improvements in the LIF system are still needed such as the quantifying the absolute pressure in the static fill case, replacing the streak camera with an ICCD camera, and reducing the background noise in the system. Further study of the nozzle at different points along the z-axis is suggested. Despite the high uncertainty the relative density measurements in the study illustrate the usage of LIF as a versatile and nondestructive testing method.

CHAPTER 7

FUTURE WORK

This study has shown the usage of LIF as a spectroscopic measuring technique to determine the density from a gas puff nozzle. In efforts to improve the efficiency of the system and a better understanding of the LIF density profiles, suggested future work is described in this section. A few tasks can still be completed with the setup using the C7700 streak camera. Investigation of gas expansion at greater distances along the z-axis is needed. The LIF measurements described in this paper were performed in the range of 4-5 mm below the nozzle. Shell-on-shell interactions are greater at z>5 mm and radial expansion is present even at supersonic speeds. Work performed by the L3 pulsed power group has shown a uniform gas distribution farther away from the nozzle [10]. Performing LIF measurements further away from the nozzle would quantify the range of a supersonic puff and its radial expansion. Due to the limitations of the C2830 streak camera interactions between shells is still not quantified. Previous studies have revealed interesting gas dynamics between the inner and outer shells [14]. As discussed in section 4.1 the technique of evacuating the inner plenum and firing the outer plenum at high pressure would reveal a single gas shell with minimized shell-on-shell interactions. A comparative map can then be constructed to illustrate the effects of shell-on-shell collisions and any outlining behavior of the gas puff.

Studies of time resolved LIF spectrum is suggested for examination. The fluorescence emission wavelength is known to be between 430-480 nm due to the observed blue/violet color of emission. However an exact wavelength of emission has yet to be determined. The fluorescence spectrum may change at

different gas pressures. Measurement of the exact photon wavelength can be used to illustrate any differences in the fluorescence or the later phosphorescence emission spectrum.

Replacing the streak camera with a multiple gate intensified CCD camera would allow measurement of phosphoresce signals below the fluorescence signal. Phosphorescence signals reveal insight into gas flow dynamics and relative intensities of the signal. LIF measurements with an ICCD camera would perceive significantly greater portion of the z-axis than shown in this study. As the gas flows downstream the slow decaying phosphorescence shows the gas puff trajectory. Multiple gates on the ICCD then capture the fluorescence and phosphorescence measurements. A 2-D flow velocity map can be created from these images by measuring the position shifts. The exhaust velocity from then the nozzle can then be accurately measured. The same small diameter pulsed UV beam is ideal for this work. However before acquiring an ICCD for image capturing, investigation in the photophysics of acetone emission is called for. Acetone excitation has a saturation limit based upon the energy of the pulsed laser beam. The UV laser used in this research is set to a fixed energy of 80 mJ and additional investment would be required to alter the laser energy. Thus is may be possible that the phosphorescence intensity is too weak for imaging due to the limitations of the laser energy.

BIBLIOGRAPHY

[1] T. F. Chang, A. Fisher and A. Van Drie. X-ray results from a modified nozzle and double gas puff z pinch. J. Appl. Phys. 1991, Vol. 69, No. 6, p. 3447.

[2] Paul Bellan. Fundamentals of Plasma Physics. Cambridge University Press, 2006.

[3] P. M. Bellan, Rev. Sci. Instrum. 73, 2900 s2002d.

[4] Eyal Kroupp personal communication

[5] B. A. Remington, R. P. Drake, and D. D. Ryutov, Rev.Mod. Phys. 78, 755 (2006).

[6] R.Hamerly. Laser Fusion: Lighting the Earth with Exploding Stars. Stanford University, 2011.

[7] N. Qi, J. Schein, J. Thompson, P. Coleman, M. McFarland, R. Prasad,M. Krishnan, B. Weber, B.Moosman, J. Schumer, D. Mosher, R. Commisso, and D. Bell, "Z-pinch imploding plasma density profile measurements using a two-frame laser shearing interferometer," IEEE Trans. Plasma Sci., vol. 30, no. 1, p. 227, Feb., 2002.

[8] E. Carate, Y. Song, A.Fisher. Determination of the mass distribution in a gas puff by laser induced fluorescence. Pulsed Power Conference, 2003. Digest of Technical Papers. PPC-2003. 14th IEEE International.

[9] Guy Rosenzweig. M.S. Thesis. Weizmann Institute of Science. 2007.

[10] D. B. Atkinson and M. A. Smith. Design and characterization of pulsed uniform supersonic expansions for chemical applications. Rev. Sci. Instrum. 1995, Vol. 66, No. 9, p. 4434.

[11] Y. Song, P. Coleman, B. H. Failor, A. Fisher, R. Ingermanson, J. S. Levine, H. Sze, E. Waisman, R. Commisso, T. Cochran, J. Davis, B. Moosman, A. L. Velikovich, B. V. Weber, D. Bell, and R Schneider,"Valve and nozzle design for injecting a shell-on-shell gas puff load into z pinch," Rev. Sci. Instrum., vol. 17, p. 3081, 2000.

[12] Thao Tran. Ph.D. Thesis. Georgia Institute of Technology. 2008.

[13] A. Lozano, B. Yip and R. K. Hanson. Acetone: a tracer for concentration measurements in gaseous flows by planar laser-induced fluorescence. Exp. in Fluids. 1992, Vol. 13, p. 369.

[14] Stephen W. Allison and William P. Partridge. Laser-Induced Fluorescence Imaging. Wiley and Sons Inc. 15 Jan 2002. DOI: 10.1002/0471443395.img060.

[15] B. H. Failor, et al. Proof-of-principle laser-induced fluorescence measurements of gas distributions from supersonic nozzles. Rev. Sci. Instrum. 2003, Vol. 74, No. 2, p. 1070.

[16] N. Qi, et al. Two-dimensional gas density and velocity distributions of a 12-cm diameter, triple nozzle argon Z-pinch load. IEEE Trans. Plasma Sci. 2005, Vol. 33, No. 2, p. 752.

[17] Pierre Gourdain personal communication.

[18] Niansheng Qi personal communication.

[19] Ronald J. Adrian, Jerry Westerweel. Particle Image Velocimetry. Cambridge University Press. 2010.

[20] Hamamatsu Photonics. High dynamic range streak camera C7700 instruction manual and test report, ver. 1.3, 2006.7, 6660-401-02.